frontiers in Earth Science

ORIGINAL RESEARCH
published: 17 December 2021
doi: 10.3389/feart.2021.795826

Late Pleistocene Climate and Dust Source From the Mobarakabad Loess–Paleosol Sequence, Northern Foothills of the Alborz Mountains, Northern Iran

Amin Ghafarpour[1]*, *Farhad Khormali*[1]*, *Xianqiang Meng*[2], *Hossein Tazikeh*[1] and *Thomas Stevens*[3]

[1]Department of Soil Sciences, Loess Research Center, Gorgan University of Agricultural Sciences and Natural Resources, Gorgan, Iran, [2]State Key Laboratory of Lake Science and Environment, Nanjing Institute of Geography and Limnology, Chinese Academy of Sciences, Nanjing, China, [3]Department of Earth Sciences, Uppsala University, Uppsala, Sweden

OPEN ACCESS

Edited by:
Kathryn Elizabeth Fitzsimmons, University of Tübingen, Germany

Reviewed by:
Charlotte Prud'Homme, University of Lausanne, Switzerland
György Varga, Hungarian Academy of Sciences (MTA), Hungary

***Correspondence:**
Amin Ghafarpour
aghafarpour@yahoo.com
Farhad Khormali
fkhormali@gau.ac.ir

Specialty section:
This article was submitted to Quaternary Science, Geomorphology and Paleoenvironment, a section of the journal Frontiers in Earth Science

Received: 15 October 2021
Accepted: 30 November 2021
Published: 17 December 2021

Citation:
Ghafarpour A, Khormali F, Meng X, Tazikeh H and Stevens T (2021) Late Pleistocene Climate and Dust Source From the Mobarakabad Loess–Paleosol Sequence, Northern Foothills of the Alborz Mountains, Northern Iran. Front. Earth Sci. 9:795826. doi: 10.3389/feart.2021.795826

Paleoclimatic investigation of loess-paleosol sequences from northern Iran is important for understanding past changes in a region highly sensitive to shifts in precipitation, and along potential routes of past human migration. Here, we present carbon and oxygen isotopic compositions of bulk carbonate ($\delta^{13}C_{bc}$ and $\delta^{18}O_{bc}$, respectively) coupled with particle size distributions of samples from the Mobarakabad section, northern Iran, to study past wind dynamics and hydroclimate. We also present new initial clay-sized Hf-Nd isotope results from key horizons in order to assess general dust sources. Variations of $\delta^{13}C_{bc}$ and $\delta^{18}O_{bc}$ values of modern soils compared to paleosols allow reconstruction of late Pleistocene–Holocene climate change in the area. Our results show severe drought during a major eolian deposition phase (EDP) after 34 ka. The thickness and PSD of the C horizon of unit 5 suggest significant shifts in loess sources and depositional environments during this EDP after 34 ka. Indeed, based on our new clay-sized Hf-Nd data, we hypothesize that the loess unit 5 might originate from the young crustal source of the Alborz and Kopet Dagh mountains. In general, the PSD of C horizons in the section is bimodal in the silt fraction and the very small, very fine clay fraction, with a mode at c. 1 μm in the modern soil and paleosols possibly produced by weathering and pedogenic processes. There also appears to be a good correlation between $\delta^{13}C_{bc}$ and $\delta^{18}O_{bc}$ values, differentiating phases of loess accumulation and paleosol formation and hence providing quantitative data for reconstructing paleoclimatic conditions in the study area.

Keywords: dust, paleosol, particle size distribution, bulk carbonate isotopes, provenance, northern Iranian loess

INTRODUCTION

Loess sediment in the mid-latitude of Eurasia provides an excellent sedimentary archive for understanding past climate and environmental changes in the continental interior (e.g., Rousseau et al., 2017, 2020; Fenn et al., 2020; Fitzsimmons et al., 2020; Költringer et al., 2020; Song et al., 2021). In northern Iran, loess deposits are found in the so-called Northern Iranian Loess Plateau (NILP) and along the northern foothills of the Alborz Mountain range (NFAM). These

deposits represent outstanding archives of past climate in a region highly sensitive to changes in hydroclimate and potentially important in past human migrations (Shoaee et al., 2021) but otherwise poorly represented by past climate records. The loess units in the area are separated by paleosols showing various development degrees, providing valuable sedimentary archives of loess accumulation, soil, and paleosol formation within the loess units (Kehl et al., 2005; Frechen et al., 2009; Kehl, 2010; Khormali and Kehl, 2011; Ghafarpour et al., 2016, 2021; Vlaminck et al., 2016, 2018; Lauer et al., 2017a; Lauer et al., 2017b; Shahriari et al., 2017; Pourmasoumi et al., 2019; Sharifigarmdareh et al., 2020; Kehl et al., 2021). These previous studies of loess–paleosol sequences in northern Iran mainly focused on dating of the deposits, particle size distributions, and paleosol formation in response to paleoprecipitation and paleopedogenic process, with little emphasis on phases of eolian deposition, meaning that additional detailed analyses of the loess units in particular are essential. In addition, there is still considerable uncertainty about the potential source(s) area of the northern Iranian loess, due to the lack of previous provenance analyses.

The particle size distribution (PSD) has proved an appropriate property of loess and eolian sediments for understanding loess sedimentary environment, eolian dynamics, and pedogenesis reconstruction (e.g., Nilson and Lehmkuhl, 2001; Vandenberghe et al., 2006; Jacobs and Mason, 2007; Prins et al., 2009; Stevens and Lu, 2009; Tripaldi et al., 2010; Vriend et al., 2011; Markovic et al., 2013; Vandenberghe, 2013; Sweeney and Mason, 2013; Schaetzl et al., 2014; Forman et al., 2014; Ujvari et al., 2016; Zeeden et al., 2016; Vandenberghe, et al., 2018; Stevens et al., 2020; Wacha et al., 2021). Most loess is dominated by medium silt-sized grains, but a proportion of fine silt and clay particles in fine-grained eolian landforms, and loess is also likely to be transported as silt- or sand-sized aggregates (Pye, 1995; Mason et al., 2003; Qiang et al., 2010; Mason et al., 2011a). The PSD of loess is the result of a combined local/regional signal of atmospheric properties (wind strength and its variations, vertical mixing) and environmental settings such as topography (Vandenberghe et al., 1997; Mason et al., 1999; Rousseau et al., 2002; Nottebaum et al., 2014), vegetation cover (Stevens et al., 2011), source distance (Ding et al., 2005; Yang and Ding, 2008), and regional aridity and/or a change in sediment availability (Forman et al., 2008; Muhs et al., 2013). Bulk loess grain size proxies such as U-ratio and "grain size indexes" (GSIs) have been commonly employed as a measure of wind strength, with application to loess depositional history in Europe, Asia, and North America (e.g., Vandenberghe et al., 1985; Vandenberghe et al., 1997; Rousseau et al., 2007; Machalett et al., 2008; Muhs et al., 2008; Antoine et al., 2009). The U-ratio represents the proportion of medium and coarse-grained silt (44–16 μm) vs. fine-sized silt (5.5–16 μm) (Vandenberghe et al., 1985), and GSI is the ratio of 20- to 50-μm/<20-μm fractions (Rousseau et al., 2002); both indices are designed to assess changes in the silt fraction and exclude larger sand particles, or in the case of the U-ratio, pedogenic clays. Kehl et al. (2005) and Kehl (2010) showed an increase in PSD from west to east and from south to north in northern Iran, coinciding with pronounced east–west and north–south gradients of modern climate from arid to subhumid.

Soil carbonate isotope studies of modern soils and paleosols have typically focused on samples collected from temperate or warm environments (e.g., Quade et al., 2007; Hough et al., 2014; Diaz et al., 2016; Gallagher and Sheldon, 2016; Ringham et al., 2016; Bayat et al., 2017; Dietrich et al., 2017). The carbon and oxygen isotope composition of pedogenic carbonate ($\delta^{13}C_{pc}$ and $\delta^{18}O_{pc}$) and land snail shell carbonate within successions of rapidly buried Quaternary soils exhibit stratigraphic trends that are interpreted to record a history of significant climate variation and provide an additional technique for investigating Quaternary climate and ecologic changes (McDonald and McFadden, 1994; Monger et al., 1998; Lechler et al., 2018; Huth et al., 2019; Újvári et al., 2019, 2021; Zamanian et al., 2021). Recent studies suggest a strong summer seasonal bias in some (Breecker et al., 2009; Passey et al., 2010; Quade et al., 2013; Huth et al., 2019) but not all pedogenic carbonates (Peters et al., 2013). The $\delta^{13}C$ values of soil carbonates are controlled by the $\delta^{13}C$ of soil CO_2, which is mainly determined by the abundance of C_3 and C_4 plants in the local ecosystem (Amundson et al., 1988; Cerling and Quade, 1993; Breecker et al., 2009). The $\delta^{13}C$ values of soil carbonates can also be affected by soil-respired CO_2 concentrations, pCO_2, and the carbon isotope value of atmospheric CO_2 (Fischer-Femal and Bowen, 2021). In addition, water availability and pCO_2 can also significantly affect the discrimination against ^{13}C during photosynthesis, which then changes the carbon isotope value of respired CO_2 (Diefendorf et al., 2010; Kohn, 2010; Schubert and Jahren, 2012; Fischer-Femal and Bowen, 2021). Soil carbonate $\delta^{18}O$ values are controlled by the oxygen isotope composition of soil water ($\delta^{18}O_{sw}$) and the temperature of mineral precipitation (Cerling and Quade, 1993; Quade et al., 2007). The $\delta^{18}O_{sw}$ values predominantly track isotope values of rainfall (Tan et al., 2017; Kelson et al., 2020), even though they can also be affected by evaporation in the near surface (e.g., Breecker et al., 2009; Huth et al., 2019). Soil carbonate $\delta^{18}O$ is thought to decrease with lower temperatures and higher elevation (Dworkin et al., 2005; Quade et al., 2011). Some authors suggested that $\delta^{13}C_{bc}$ in loess represents a mixed signal derived from both detrital carbonate and authigenic pedogenic carbonate (Ning et al., 2007; Liu et al., 2011; Koeniger et al., 2014), and the effects of multiple formation times on bulk soil carbonate isotope composition should also be considered (Burgener et al., 2016). Also, Zamanian et al. (2021) studied isotopic signatures of different types of carbonates in the Nussloch paleosol-loess sequence in Germany, and they excluded the stable isotope composition of bulk carbonate for reconstructing the local paleoenvironment because the bulk carbonates in the section were detrital materials from the diagenetic conditions of carbonates in the deflation area.

$\delta^{13}C_{bc}$ values have been shown to be an indicator of paleovegetation density in response to the intensity of the Asian summer monsoon in arid parts of the Chinese loess plateau (Rao et al., 2006). In addition, some investigations on modern ecosystems have identified that the increase in mean annual precipitation (MAP), to which soil humidity is directly related, influences vegetation density and together, and these factors cause a depletion in $\delta^{13}C_{bc}$ and $\delta^{13}C_{pc}$ values in the

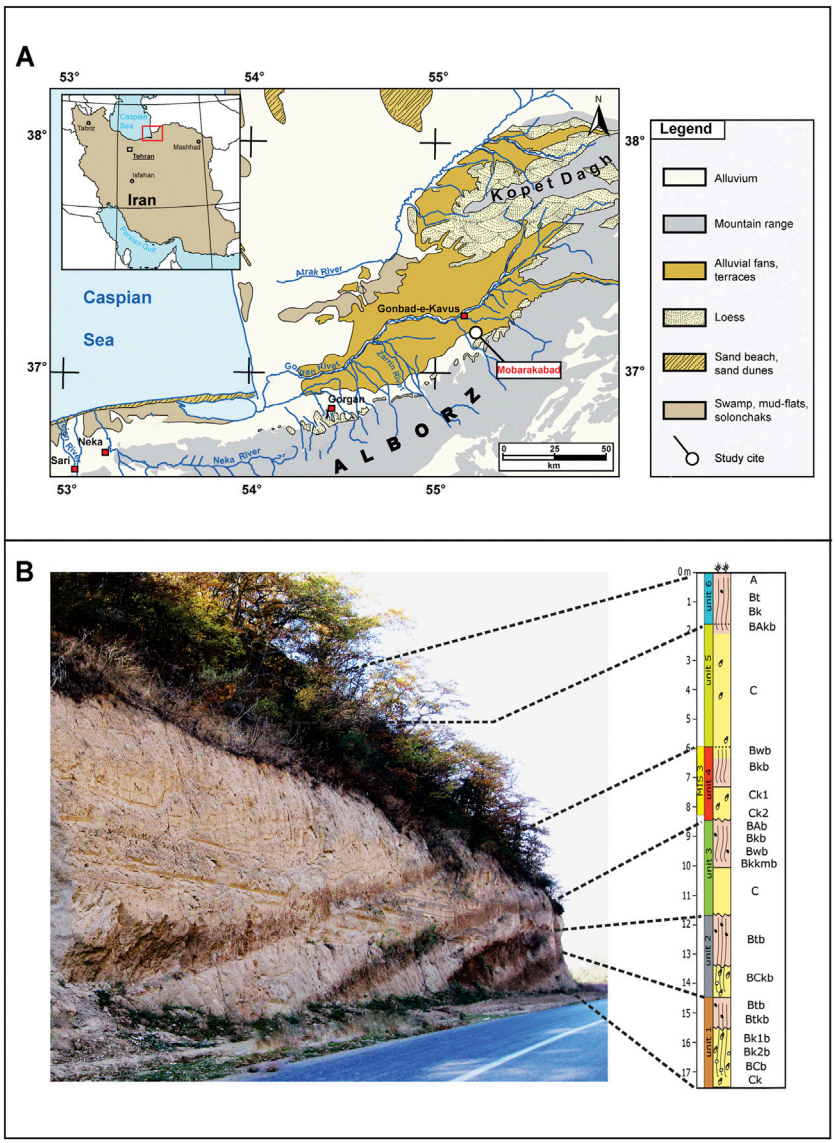

FIGURE 1 | (A) Map of north Iran showing the locations of the study site and the occurrence of loess deposits supplemented by other geomorphological features in the region (after Kehl et al., 2021). **(B)** Photo overview and stratigraphic section of Mobarakabad, showing bedding characteristics, buried soils (paleosols) with recognized horizons (**Figure 3** for legend). The total thickness of the section is about 17 m, and it contains six loess units separated by paleosols. Section location: Mobarakabad (37° 09′ 32″ N, 55° 18′ 14″ E).

northwestern Chinese loess plateau (CLP). Chinese loess $\delta^{13}C_{bc}$ variation therefore likely reflects the regional precipitation change and therefore can be regarded as a sensitive proxy for the summer monsoon intensity (Liu et al., 2011; Sun et al., 2015). Recently, Khormali et al. (2020) investigated δ^{13} C_{bc} and δ^{18} O_{bc} as well as $\delta^{13}C_{pc}$ and $\delta^{18}O_{pc}$ and organic carbon from modern soils and paleosols in northern Iran along a west to east and south to north precipitation gradient. They concluded that $\delta^{13}C_{bc}$ and $\delta^{18}O_{bc}$ values showed a significant relationship with MAP, over the range from 200 to approximately 750 mm/yr, and also suggested a summer bias in carbonate nodule formation in the area. This development opens up an excellent opportunity to reconstruct hydroclimate in northern Iran and yield new insights into climate variability and forcing in the region.

While past climate records based on isotopic and particle size parameters are still much needed to refine the picture of Quaternary climate change from loess in northern Iran, the provenance of loess in this area has not been studied previously. The clay-sized Hf-Nd isotopic composition of dust has been successfully used as a tool for aerosol/dust source discrimination (Pettke et al., 2002; Aciego et al., 2009; Lupker et al., 2010; Pourmand et al., 2014; Ujvari et al., 2015; Zhao et al., 2014, 2015), based on the fact that radiogenic isotopes of these elements differ in source rocks of different ages and weathering histories. Compared with the detailed provenance studies of

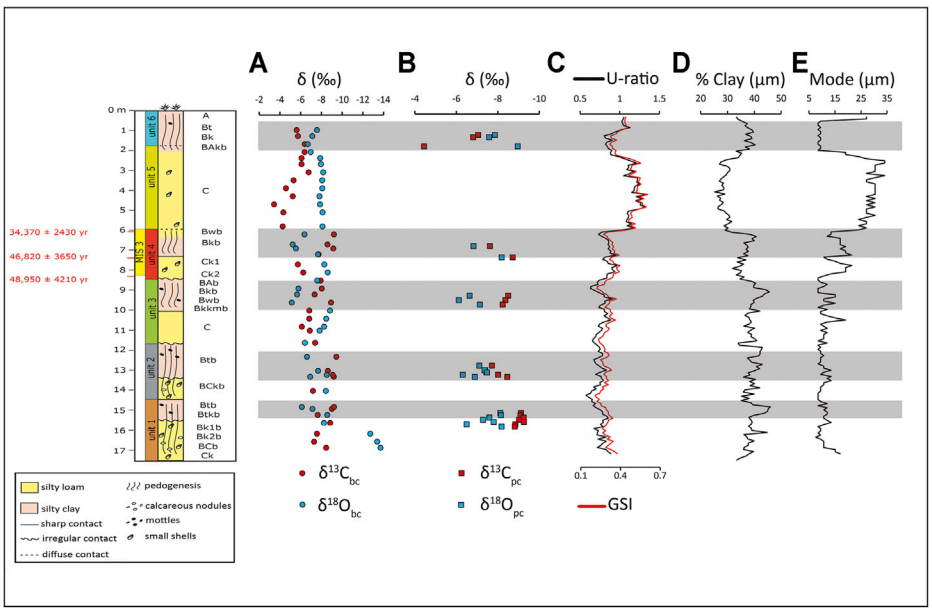

FIGURE 2 | Stratigraphic column for Mobarakabad along with trends of **(A)** $\delta^{13}C_{bc}$ and $\delta^{18}O_{bc}$, **(B)** $\delta^{13}C_{pc}$ and $\delta^{18}O_{pc}$ (Khormali et al., 2020), **(C)** U-ratio and GSI, **(D)** clay (<5.5 μm), **(E)** mode. Note in the stratigraphic column, the capital letters A, B, and C represent the master horizons of loess units (Soil Survey Staff, 2014). Lowercase letters are used as suffixes to designate specific subordinate distinctions within master horizons. The suffix symbol meanings are as follows: b: buried genetic horizon; k: accumulation of secondary carbonates; kk: engulfment of the horizon by secondary carbonates; m: pedogenic cementation; t: accumulation of silicate clay; and w: development of color or structure (Soil Survey Staff, 2014).

aerosol/dust in Greenland (Lupker et al., 2010), Mongolian Plateau (Zhao et al., 2015), CLP (e.g., Zhao et al., 2014), Carpathian Basin (Újvári et al., 2012), and North Africa (e.g., Zhao et al., 2018), the provenance of northern Iranian loess has not been investigated so far and lacks analyses of multiple clay-sized Hf-Nd isotopic compositions. Dust provenance to loess deposits is especially important to constrain in order to understand past sediment routing processes, dust transport, and a possible link to climate change.

This study presents $\delta^{13}C_{bc}$, $\delta^{18}O_{bc}$, and PSD of the late Pleistocene loess–paleosol sequences at Mobarakabad in northern Iran (**Figure 1A**), in order to reconstruct late Pleistocene hydroclimate and eolian processes in the region. Also, we report the first clay-sized Hf-Nd isotopic composition for northern Iranian loess, focusing on the three upper loess units at the section, which accumulated since middle MIS 3. Our aims were to 1) assess the feasibility of using $\delta^{13}C_{bc}$ and $\delta^{18}O_{bc}$ to reconstruct paleoenvironment at the study section, 2) demonstrate how the PSD of the loess–paleosol sequence reflects paleoclimate changes, and 3) make a first general preliminary assessment of potential source(s) of loess on the northern foothills of the Alborz Mountain range since late MIS 3.

GEOGRAPHIC SETTING

The study area is characterized by seasonal rainfall variation, with high precipitation amounts from October to March, dropping sharply in summer when the air temperature reaches its peak in July–August. The section at Mobarakabad is located on the NFAM and lies 310 m above sea level, with forest vegetation cover. The modern climate at Mobarakabad is characterized by ~680 mm MAP and with a mean annual air temperature (MAAT) of 16.5°C. The 17-m-thick section at Mobarakabad contains six loess units separated by paleosols (**Figure 1B**). The uppermost unit (unit 6) is the modern soil that formed under forest vegetation and is classified as a Calcic Argixeroll in the U.S. Department of Agriculture (USDA) soil taxonomic system (Soil Survey Staff, 2014). Unit 5 is ~4 m thick and primarily reflects eolian deposition and contains some shells of mollusks. Unit 4 lies below this, 6–8 m below the surface. The upper 1 m of unit 4 is a pedogenically altered, light brown soil with secondary calcium carbonate (Bwb and Bkb horizons). Furthermore, small shells of mollusks are detected in the Ck1 and Ck2 horizons of this unit (**Figure 2**). The underlying unit 3 exhibits BAb, Bkb, Bwb, Bkkmb, and C horizons and contains Fe mottles, and at the top of the unit, a 5- to 7-cm weak, buried organic-rich horizon is present (**Figure 2**). The uppermost 1.5 m of unit 2 is a well-developed paleosol (Btb) that shows clear signs of secondary accumulation of clay containing and Fe mottles based on visual observation in the field. The BCkb horizons of unit 2 reflect eolian depositional phases composed of detrital carbonate with small shells of mollusks (**Figure 2**). The lowermost unit (unit 1) lies at a depth of ~14.5 below the surface and is mostly pedogenically altered, hosting well-developed Btb and Btkb horizons. The lower 2.5 m of unit 1 contains Bk1b, Bk2b, BCb, and Ck horizons, containing pedogenic carbonate with small shells of mollusks (**Figure 2**).

METHODS

Sampling

A total of 164 samples were taken in 10-cm intervals for particle size measurements down section, while 40 samples were taken from the modern soil, C horizons, and paleosols for carbon and oxygen isotope analyses of bulk carbonates. In addition, four samples from the Bt and Bk horizons of the modern soil (unit 6), C horizon of unit 5, and Bk horizon of unit 4 were selected for clay-sized Hf-Nd isotopic measurements.

Particle Size Measurements

All samples were treated using 0.1 N HCl and 10% H_2O_2 before instrument measurement to remove carbonate and organic matter, respectively. After adding deionized water, sample suspension was left for 48 h prior to pipetting, to remove acidic ions. After that, the samples were dispersed with 10 ml of 30% $(NaPO_3)_6$ and placed in an ultrasonic vibrator for 10 min prior to particle size measurements. Each sample was measured three times repeatedly in a Mastersizer 2000 Laser Particle Analyzer at the Ministry of Education Key Laboratory of Surficial Geochemistry, Nanjing University. A constant of 1.33 was used for the refractive index of dispersant water, while a 1.52 refractive index was used for the solid phases (Özer et al., 2010), and an absorption index of 0.1 was applied. The default ideal range of obscuration on the Mastersizer 2000 (10–20%) is adopted as a working obscuration target for our standard operating procedure. As an assessment of measurement uncertainties, it must be noted that the applied optical parameter settings in laser diffraction may have considerable effects on the grain size results, in particular for the clay fractions (Varga et al., 2019a). At the same time, the clay size content of sediments is typically underestimated by the laser diffraction method in comparison with other methods such as pipette analyses (Beuselinck et al., 1998; Mason et al., 2003; Polakowski et al., 2014). Konert and Vandenberghe (1997) suggested the clay-silt break be set at 8 μm for comparison with traditional, that is, pipette particle size analysis. Our data have suggested better correlations between laser diffractometry and the pipette method (Ghafarpour et al., 2016) when the clay-silt break is set at 5.5 μm. Therefore, we used a 5.5-μm clay-silt break in this study. (For further discussion on the principles and application of laser diffractometry for particle size characterization, see, e.g., Mason et al. (2011b), Miller and Schaetzl (2012), and Varga et al. (2019b).)

$\delta^{13}C_{bc}$ and $\delta^{18}O_{bc}$

The samples were ground to <75 um; ~200 mg of powdered sample was reacted directly with 100% phosphoric acid for 20 min at 70°C to produce carbon dioxide. Carbon dioxide was gathered and analyzed with MAT-253 at the Nanjing Institute of Geology and Palaeonotology, Chinese Academy of Sciences. Carbon and oxygen isotope compositions were measured and normalized against international standards (NBS-19). Isotope values are given in per mil (‰) as δ values:

$$\delta\,(‰) = \left[\left(R_{Sample}/R_{Standard}\right) - 1\right] \times 1000,$$

where R is the ratio of the heavier to the lighter isotopes of carbon and oxygen ($^{13}C/^{12}C$, $^{18}O/^{16}O$). All δ values are expressed against V-PDB (Vienna Peedee Belemnite). The standard deviation is less than 0.08 and 0.03‰ for $\delta^{18}O$ and $\delta^{13}C$, respectively.

Hf-Nd Isotope Measurements of Units 4-6

Hf and Nd isotopic analyses followed the procedures described by Zhao et al. (2014). To isolate the clay-sized silicate mineral fraction for Hf analysis, organic matter and carbonate were removed. Organic matter was removed with excess hydrogen peroxide (30%) overnight and then a decarbonation step was carried out using excess 1 M acetic acid for 10 h in order to eliminate the influence of secondary carbonate on Hf isotopic composition. The samples were subsequently rinsed at least three times with MilliQ water to completely remove major ions and soluble salts. Different fractions were extracted by sieving the ultrasonically dispersed samples in mesh with MilliQ water, and the 2-μm particles were separated based on Stokes' law and then were recovered by centrifuging. The samples were subsequently rinsed at least three times with MilliQ water to completely remove major ions and soluble salts. The Hf-Nd isotopic ratios of the extracted clay-sized fractions were measured with a Thermo Fisher Scientific Neptune MC-ICP-MS at the State Key Laboratory for Mineral Deposits Research, Nanjing University. These samples were prepared as follows: first, sample digestion; 100 mg of the dry silicate residue was totally dissolved with HF–$HClO_4$ mixture in steel jacketed autoclaves at 180 ~200°C for 72 h, while 100 mg of clay-sized fractions were digested with a mixture of HF–$HClO_4$ 110~140°C for 72 h. The second step is purification for Hf and Nd with ion chromatography. The Hf analysis used a modified method of Yang et al. (2010), which includes dissolving the samples in an HF–HClO4 mixture and separation by chromatographic extraction using a cation exchange resin, Bio-Rad 50WX8 resin + Eichrom® Ln-Spec resin. Hafnium was separated from the matrix by ion-exchange procedures using Eichrom® Ln-Spec resin. The details of the analytical procedure for the Hf isotopic measurement are published elsewhere (Yang et al., 2010). Nd was then separated and purified by ion-exchange procedures (Pu et al., 2005). All chemical digestion and purification were carried out in a Class 100 ultraclean laboratory. $^{179}Hf/^{177}Hf$ was normalized to 0.7325, and $^{143}Nd/^{144}Nd$ was normalized to 0.7219. The analytical blank was <60 pg for Nd and <60 pg for Hf. Reproducibility and accuracy of the Hf and Nd isotopic analyses were periodically checked by running the standards, Nd (JNDi-1) and Hf (MC-475) every two sample runs. The mean standard $^{143}Nd/^{144}Nd$ value was 0.511840 ± 8 (2σ external standard deviation, n = 6), and the mean standard $^{176}Hf/^{177}Hf$ value was 0.282160 ± 8 (2σ external standard deviation, n = 15). The observed natural variability in Hf and Nd isotopic composition is small and usually expressed in εHf and εNd notations, which are deviations from the Chondritic Uniform Reservoir (CHUR, $^{176}Hf/^{177}Hf$ = 0.282785 and $^{143}Nd/^{144}Nd$ = 0.512630) and calculated using the equations of Bouvier et al. (2008) as follows:

$$\varepsilon Hf = 10^4 \times \left[{}^{176}Hf/{}^{177}Hf_{sample} - {}^{176}Hf/{}^{177}Hf_{CHUR}\right]/{}^{176}Hf/{}^{177}Hf_{CHUR},$$

$$\varepsilon Nd = 10^4 \times \left[{}^{143}Nd/{}^{144}Nd_{sample} - {}^{143}Nd/{}^{144}Nd_{CHUR}\right]/{}^{143}Nd/{}^{144}Nd_{CHUR}.$$

RESULTS AND DISCUSSION

$\delta^{13}C_{bc}$ and $\delta^{18}O_{bc}$ Results

Carbonate $\delta^{18}O$ and $\delta^{13}C$ records and particle size parameters of the Mobarakabad section are shown in **Figures 2A–E**. The samples show $\delta^{13}C_{bc}$ ranging from −9.4 to −3.4‰ (mean value = −7.1‰) and $\delta^{18}O_{bc}$ ranging from −13.7 to −5.1‰, with a mean value of −7.8‰. Comparison of organic and carbonate $\delta^{13}C$ values of samples reveals that both pedogenic and bulk carbonates are enriched 14.5–16.5‰ with respect to associated organic matter, suggesting that organic matter and carbonate are cogenetic (Cerling et al., 1989). In units 1–5, $\delta^{13}C_{bc}$ values decrease with increasing pedogenesis and vegetation cover from loessic C horizons to the paleosols (**Figure 2A**). Additionally, the vegetation in the paleosols of the section is dominated by C_3 plants, with a mean $\delta^{13}C$ value of soil organic matter (−23.6‰) (Khormali et al., 2020). Thus, $\delta^{13}C_{bc}$ values of paleosols are very sensitive to changes in the precipitation-controlled vegetation density and can serve as a reliable proxy of paleoprecipitation. During paleosol formation (interglacials and/or interstadials) in units 1–5, enhanced precipitation can result in increased soil moisture and biomass, strong soil respiration, and high pCO_2, leading to the depleted carbonate $\delta^{13}C$ values in the paleosols (Cerling et al., 1989; Quade et al., 1989; Liu et al., 2011).

The Bkb and BCb horizons of unit 1 produced an average $\delta^{18}O_{bc}$ value of ~ −13.3‰ and an average $\delta^{13}C_{bc}$ value of ~ −8.3‰. In contrast, the average $\delta^{13}C_{bc}$ and $\delta^{18}O_{bc}$ values of upper Btb and Btkb horizons in unit 1 are ~ −9 and ~−7.7‰, respectively. Additionally, the average $\delta^{13}C_{pc}$ and $\delta^{18}O_{pc}$ values in the Btb and Btkb horizon of unit 1 are ~ −8.8 and ~−7.8‰, respectively (**Figure 2B**). Therefore, lower $\delta^{18}O_{bc}$ values of Bkb and BCb horizons relative to $\delta^{18}O_{bc}$ and $\delta^{18}O_{pc}$ values of upper Btb and Btkb horizons in unit 1 suggest that the Bkb and BCb horizons record colder periods of carbonate formation than the Btb and Btkb horizons. Also, a (~5.5‰) increase in the $\delta^{18}O_{pc}$ values of the Btb and Btkb horizons compared to the Bkb and BCb horizons in unit 1 reflects significant evaporative ^{18}O enrichment at shallow soil depths. This observation is in line with other studies suggesting that evaporation affects oxygen isotope values at shallow soil depths (e.g., Quade et al., 1989; Breecker et al., 2009; Stevenson et al., 2010). Thus, we infer that pedogenic carbonates in unit 1 could initially form at the time of the deepest wetting front penetration into the soil during the summer season when soil moisture levels are low (Quade et al., 1989; Stevenson et al., 2010). Furthermore, it is the maximum wetting front that fixes the $\delta^{18}O$ values of the soil carbonates, and therefore, no marked difference between $\delta^{18}O_{pc}$ values compared to $\delta^{18}O_{bc}$ is seen in the paleosol of unit 1.

The $\delta^{18}O_{bc}$ values of the C horizons of units 2–4 are about −7 to −8‰, and the $\delta^{18}O_{bc}$ values of paleosols of units 2–4 range from ~−5.1 to ~ −8.3‰, suggesting a positive shift of ~2–3‰ in $\delta^{18}O_{bc}$ values of these paleosols compared to underlying C horizons (**Figure 2A**). The mean $\delta^{18}O_{bc}$ values of paleosols of units 2–4 (−7.2‰) are similar to mean $\delta^{18}O_{pc}$ values (−7.4‰) of these paleosols, showing no shift in the seasonality throughout the time of accumulation of carbonate nodules in the paleosols of units 2–4. This may suggest that carbonates in the paleosols of units 2–4 formed over the same time periods during the summer seasons when soil temperature and soil water evaporation are high, and so the major driving variables behind the $\delta^{18}O_{bc}$ values might be the temperature of carbonate formation.

The average of $\delta^{13}C_{bc}$ (~−5.3‰) with the maximum values of −3.4‰ of the C horizon of unit 5 is higher than that of the other loessic C horizons. The inferred timing of eolian phases of unit 5 is after 34 ka (Ghafarpour et al., 2017), and the average pH value of the C horizon of this unit is about 7.8 with relatively high carbonate contents (~20%) (Ghafarpour et al., 2016). When vegetation cover is low, due to aridity, the soil zone CO_2 becomes mixed with atmospheric CO_2, which has a more positive value. Furthermore, high rates of soil moisture evaporation result in the degassing of CO_2, preferentially of the lighter $^{12}CO_2$, therefore also resulting in higher δ^{13} C values in the soil carbonates (Dever et al., 1987; Candy et al., 2012; Gallant et al., 2014). Therefore, high $\delta^{13}C_{bc}$ with a pH of 7.8 in the C horizon of unit 5 probably reflects a period of increasing loess accumulation accompanied by an arid environment.

The $\delta^{18}O$ value of rainfall ($\delta^{18}O_{mw}$) can be used to predict $\delta^{18}O_{sw}$ values and determine how they interact on an ecosystem scale (Quade et al., 1989; Stevenson et al., 2010; Hough et al., 2014). In the modern soil, the calculated $\delta^{18}O_{sw}$ from which the soil carbonate formed was −8.3 to −7.1‰ (Kim and O'Neil, 1997), consistent with the local rainfall $\delta^{18}O_{mw}$ value (−8.2‰). This suggests that the Bk horizon of modern soils at ~ 130 cm depth did not undergo significant dewatering by evaporation prior to pedogenic carbonate formation, and thus, the $^{18}O_{pc}$ values (−8.1‰) of Bk horizons have not been influenced by the evaporation of soil water. In the modern soil, $\delta^{13}C_{bc}$ and $\delta^{13}C_{pc}$ are higher than $\delta^{18}O_{bc}$ and $\delta^{18}O_{pc}$ values, respectively. This trend in modern soil differs significantly from that shown in paleosols in which $\delta^{13}C_{bc}$ and $\delta^{13}C_{pc}$ values are lower than $\delta^{18}O_{bc}$ and $\delta^{18}O_{pc}$ values, respectively (**Figure 2A**). The observed shift in average $\delta^{13}C_{pc}$ values from paleosols (−8.5‰) to modern soil (−6.1‰) suggests that the paleosols $\delta^{13}C_{pc}$ values were ~2.5‰ lower than those of the modern soil. Additionally, the $\delta^{13}C_{pc}$ values of the modern soil of Mobarakabad are similar to the average $\delta^{13}C_{pc}$ values of loessic modern soils (−6.2‰) in the NFAM with forest cover, reported in Khormali et al. (2020). Furthermore, the mean $\delta^{13}C$ values of soil organic matter (−23.6‰) of the paleosols in Mobarakabad (Khormali et al., 2020) are within the same range as the $\delta^{13}C$ values of modern soil organic matter, indicating a C_3-dominated environment for both paleosols and the modern soil of Mobarakabad. Therefore, we

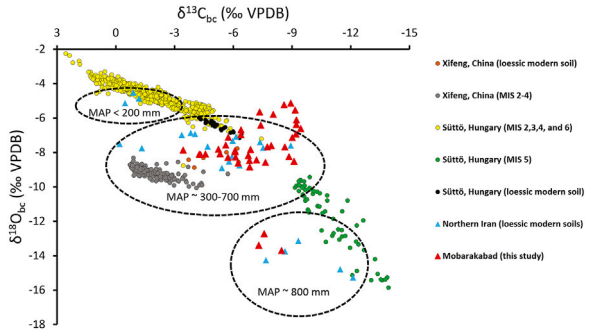

FIGURE 3 | Comparison of $\delta^{13}C_{bc}$ and $\delta^{18}O_{bc}$ values of loess–paleosol samples of Mobarakabad (this study) with $\delta^{13}C_{bc}$ and $\delta^{18}O_{bc}$ of loessic modern soils in northern Iran (Khormali et al., 2020) and loess–paleosol sequences at Xifeng in China (Luo et al., 2020) and at Sütto in Hungary (Koeniger et al., 2014). Note that dashed ovals show mean annual precipitation of the loessic modern soil sections in northern Iran, which correspond to ranges of isotope data from the same sections Khormali et al. (2020).

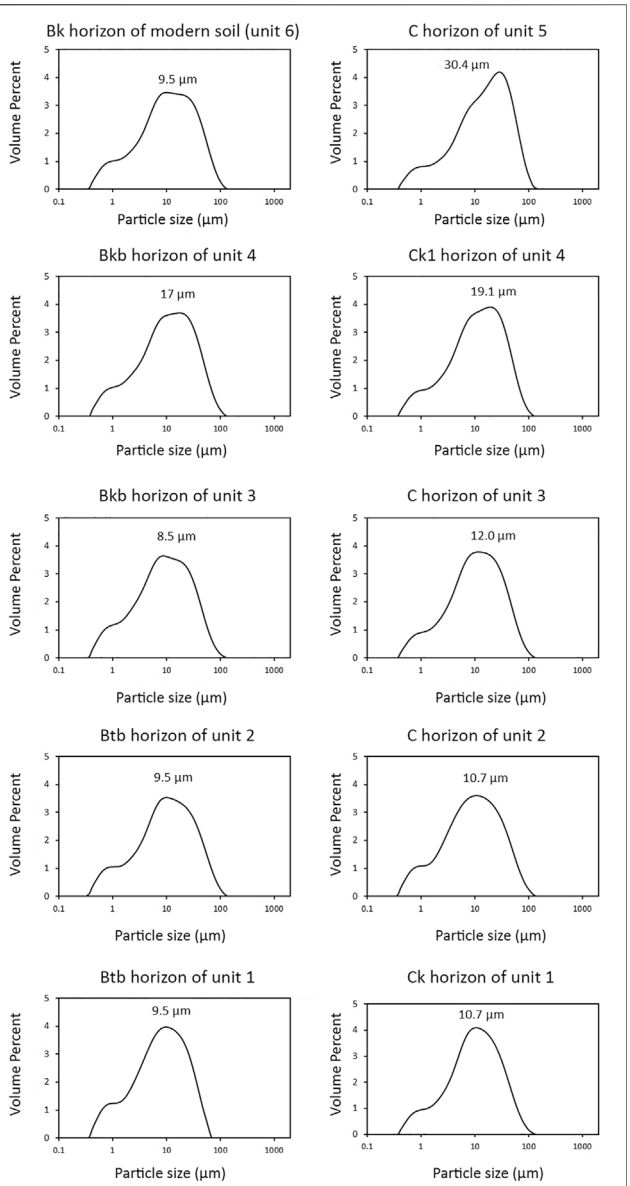

FIGURE 4 | PSD curves with the modal sizes of modern soil, C (k) horizons, and paleosols (Bkb and Btb horizons) at the study section.

inferred a ~2.5‰ increase in $\delta^{13}C_{pc}$ values of the modern soil of Mobarakabad and loessic modern soils in northern Iran (Khormali et al., 2020), as compared to paleosols of Mobarakabad section, might result from a drier climate in Holocene, as compared to the paleosol formation periods in late Pleistocene in the NFAM. In contrast, the similarity in average $\delta^{18}O_{pc}$ values of both the modern soil and paleosols in Mobarakabad (−7.3‰) with the average $\delta^{18}O_{pc}$ values of loessic modern soils in the NFAM (−7.4‰) may reflect no shift in the source of late Pleistocene-to-Holocene regional precipitation in the NFAM.

A comparison $\delta^{18}O_{bc}$ and $\delta^{13}C_{bc}$ values of Mobarakabad samples with those of loessic modern soils in northern Iran (Khormali et al., 2020), and the loess–paleosol sequences at Xifeng in China (Luo et al., 2020) and at Sütto in Hungary (Koeniger et al., 2014) are shown in **Figure 3**. This illustrates that the $\delta^{18}O_{bc}$ and $\delta^{13}C_{bc}$ values of most Mobarakabad samples match with $\delta^{18}O_{bc}$ and $\delta^{13}C_{bc}$ values of those loessic modern soils in northern Iran (MAP ~300–700 mm), Xifeng in China (MAP = 480 mm), and Sütto in Hungary, each receiving ~600–650 mm of annual precipitation. Interestingly and in contrast, the $\delta^{18}O_{bc}$ values of Bkb and BCb of unit 1 at Mobarakabad are in the range of loessic modern soil isotope values in northern Iran, where MAP is ~800 mm and MIS 5e loess in Hungary (**Figure 3**). In addition, by comparing loess units at Mobarakabad, including the OSL ages of unit 4, with stratigraphy and previously published luminescence ages from other sections at NFAM, this unit 1 at Mobarakabad correlates well with MIS 5e (*Particle Size Parameters of Loess Units*). Corroborating this assignment, based on magnetic depletion in the paleosol of unit 1 at Mobarakabad, Ghafarpour et al. (2021) concluded that the paleosol formation was accompanied by high (winter) rainfall in which dissolution of pedogenic maghemite–magnetite occurred. As such, one way of explaining these observations is high rainfall in winters, probably in MIS 5e, followed by dry and hot summers in which evaporative soil water loss predominates with little meteoric recharge, resulting in enriched $\delta^{18}O_{bc}$ and $\delta^{18}O_{pc}$ values of the upper horizons (Btb and Btkb) compared to those of Bkb and BCb horizons in unit 1 (**Figure 2A**).

Our dataset suggests that the $\delta^{13}C_{bc}$ and $\delta^{18}O_{bc}$ values of the loess–paleosol sequences at Mobarakabad are well correlated with changing phases of increased eolian sedimentation and periods of pedogenesis recorded in the loessic C horizons and paleosols, respectively, and most likely reflect the regional precipitation change. We find that both $\delta^{13}C_{bc}$ and $\delta^{18}O_{bc}$ values decrease with increasing rainfall, pedogenesis, soil humidity, and C_3 biomass, from the loessic C horizons to paleosols. However, it is also essential to take into account that any change in the source of loessic detrital materials in the modern soil reflects the conditions

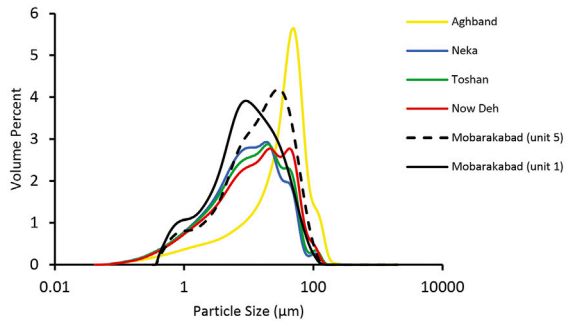

FIGURE 5 | PSD curves of C horizons of unit 1 (black line) and unit 5 (dashed line) at Mobarakabad in comparison with least weathered loess at Toshan (green line) (Vlaminck et al., 2016), Now Deh (red line), and Neka-Abelou (blue line) sections (Kehl et al., 2021) on the NFAM. The yellow line represents PSD of a loess sample from Aghband in the NILP (Lauer et al., 2017a) (see text for discussion).

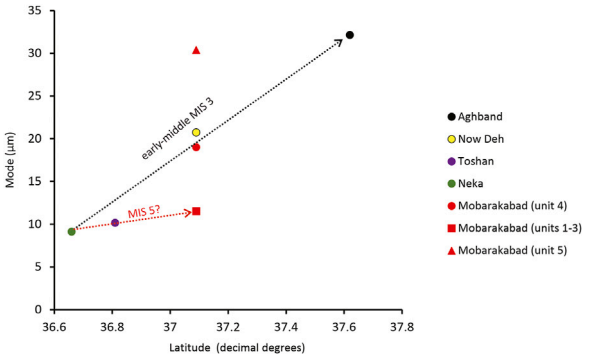

FIGURE 6 | Relationship between the mode size of loessic C horizons and the latitude of Mobarakabad as well as the mode grain size of loess–paleosol sequences located along the NFAM (Vlaminck et al., 2016; Kehl et al., 2021), supplemented by data from the Aghband section (Lauer et al., 2017a) in the NILP. Note that with increasing latitude, the mode size of loess from early to middle MIS 3 increases ($r^2 = 0.98$), but it appears that there is a weaker trend in the mode size of loess samples in the sections at the NFAM within MIS 5 (see text). There is a noticeable anomaly in the C horizon of unit 5 (red triangle) at Mobarakabad that is accumulated after 34 ka (see text for discussion).

of $\delta^{13}C_{bc}$ and $\delta^{18}O_{bc}$ values in the deflation area, rather than local environmental conditions.

Particle Size Parameters of Loess Units

All the sample particle size distributions from the C horizons of the section are bimodal in the silt fraction. One mode lies at ca. 19 μm, but all the distribution curves show a broad top which consists of two modes, with the second one somewhat coarser at ca. 35 μm. The latter mode dominates only in the C horizons of unit 5. The C and Ck horizons of units 1–3 show a fine modal particle size of 10.7–12 μm, and the Ck1 and Ck2 horizons of unit 4 show a bimodal distribution with a modal particle size of 19.1 μm (**Figure 4**). These fine-grained loess types approximately correspond to the "subgroup 1. c.," with the modal diameter ranging from 4 to 22 μm classified by Vandenberghe (2013). This subgroup is interpreted to be transported and deposited as background dust transported in high-suspension clouds over long distances continuously over time and incorporated in the high-level westerlies (Pye, 1995; Sun et al., 2002; Vandenberghe et al., 2018). Under such a scenario, it is therefore possible that the C horizon samples include loess transported over long distances (c. 10.7–12 μm mode) and loess transported over a short distance (c. 35 μm mode) by lower level suspension. Furthermore, the very small fraction of fine clays with mode at c. 1 μm in the loessic C horizons suggests an origin from high-level background dust mixed with a small amount of clay which might originate from sources that consist of very fine particles such as a very fine-grained alluvium. However, we cannot exclude the possibility that the fine-grain clay-sized particles are also partly a product of weathering or transported as aggregates in lower-level suspension clouds over shorter distances of 10–100 s of km, as discussed previously.

The C horizon of unit 5 is characterized by the lowest clay content (26%) and highest U-ratios (1.3) as well as GSI (0.6), with a mode size around 34 μm, representing the coarsest segment of the section (**Figures 2C–E**, **4**). This is exceptionally coarse for the profile and dominates the changes in grain size parameters with depth at the site; the implications will be discussed later. In units 1–3, the modal values of loessic C horizons (10.7–12 μm), U-ratio (~0.8), and GSI (~0.3) are lower than those of unit 5. Also, the average clay content of the loessic C horizons of units 1–3 (38%) is higher than of loessic C horizon of unit 5 (26%). These trends may suggest that the dynamics of the silt population is also reflected in the clay-sized fraction. Therefore, we interpret the increase in clay content of the loessic C horizons of units 1–3 as resulting from source(s) with very fine-grained alluvium and/or were probably carried in high suspension clouds at least hundreds of kilometers (*Comparison With Other Northern Iranian and Global Loess Records*), rather than being produced by weathering or pedogenic process. This may suggest that the % of clay is at least partly influenced by eolian processes, rather than reworking, as in theory, the U-ratio at least ought to reflect changes in the eolian dynamics independent of postdepositional pedogenesis (Vandenberghe et al., 1985). As such, we generally interpret the changes in grain size parameters in the loessic C horizons of the Mobarakabad section as showing more intensive eolian dynamics during phases of loess deposition as than periods of pedogenesis and soil formation, especially higher wind speeds and/or relatively greater coarse sediment availability during loess forming periods. The impact of possible source changes is discussed in *Comparison With Other Northern Iranian and Global Loess Records*.

In marked contrast, the developed Bk(b)-, Bt(b)-, and Btk(b) horizons of the modern soil and paleosols exhibit clay (<5.5 μm) proportions between 38.5 and 45.5% (**Figure 2D**). These buried horizons in modern soil and paleosols have clearly been affected by pedogenic processes, and their high clay content (with an increase in pedogenic smectite content) is the result of weathering and clay illuviation (Ghafarpour et al., 2016). Therefore, we argue that in the modern soil and paleosols, the dominant mode at c. 8.5–9.5 μm, with a secondary one in very fine clay fraction (c.

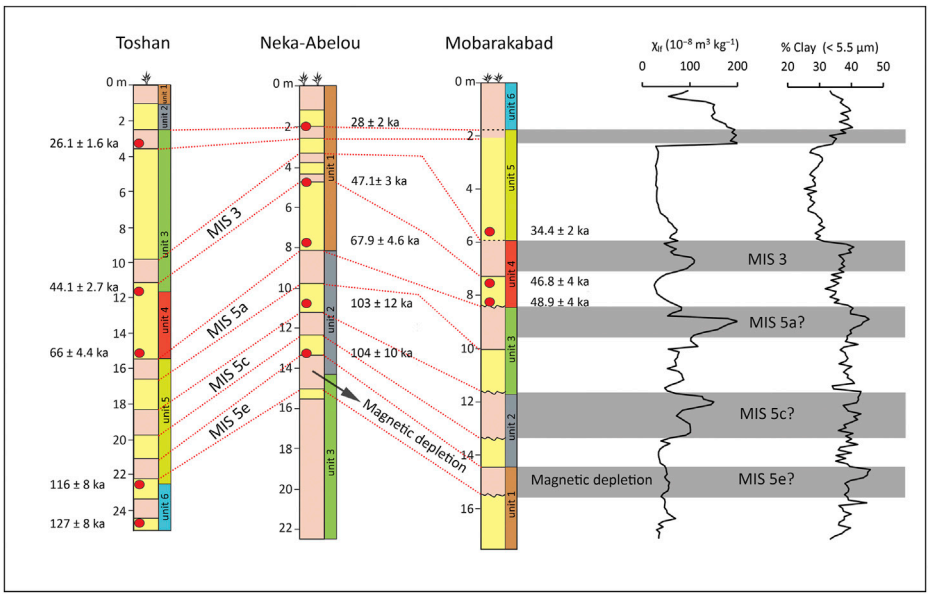

FIGURE 7 | Correlation among loess (in yellow) and paleosols (in pink) of the loess–paleosol sequences located in NFAM based on patterns of magnetic susceptibility (Ghafarpour et al., 2016), clay variations (this study), and OSL ages (Ghafarpour et al., 2017) at Mobarakabad and associated luminescence ages (red circles) of Toshan and Neka-Abelou sections (see Vlaminck et al., 2016; Kehl et al., 2021).

1 μm), was almost certainly produced by pedogenic processes and clay illuviation (Mason et al., 2003; Stevens et al., 2011) but potentially mixed up with clay (illite and kaolinite) derived from background dust input.

Comparison With Other Northern Iranian and Global Loess Records

One possible way to identify local effects on PSD is to compare the spatial patterns of loess thickness and PSD over a depositional area (e.g., Muhs et al., 1999, 2008; Mason, 2001; Mason et al., 2003) as the trends may provide insights into sediment transport pathways or distance from the source, availability of sediment, and sedimentation rate. Furthermore, these comparisons allow wider patterns to be identified that are independent of local topographic or proximal source influences. Previous studies in northern Iran defined the median particle size as 9.12–11 μm for least weathered loess at Neka-Abelou and Toshan sections (**Figure 5**) on the NFAM (Vlaminck et al., 2016; Kehl, et al., 2021). In particular, the modes of the C horizons of units 1–3 (10.7–12 μm) at Mobarakabad are comparable with the modal values of the loess (~11 μm) in unit 5 at Toshan (**Figure 6**) and also with the mode size of loess in unit 3 (~10.5 μm) at Neka-Abelou (**Figure 6**), both forming during MIS 5 (Lauer et al., 2017b; Kehl et al., 2021) (**Figure 7**). This consistency implies similar source and dust transport dynamics for these loess sediments. By comparing the OSL ages (unit 4), magnetic susceptibility, and clay variations of loess units at Mobarakabad with the previously published results from luminescence dating of Neka-Abelou and Toshan sections, we suggest that the units 1–3 at Mobarakabad correlate well with MIS 5 (**Figure 7**), supporting the assignment based on the isotopic analyses above. Therefore, we postulate that the similarity between modal peaks of MIS 5 loess at Mobarakabad, Neka-Abelou, and Toshan sections suggests that the loess was probably carried some hundreds of kilometers over a wider area from its source(s) and that the source material consisted of very fine particles (such as a very fine-grained alluvium). To a great extent, therefore, the fine MIS 5 loess at Mobarakabad and other sites on the NFAM would be consistent with transport in high suspension clouds throughout the year over (relatively) large distances, at least under the model of Vandenberghe (2013). We do however agree that luminescence ages from units 1–3 at Mobarakabad are needed to support these interpretations.

By contrast, the strong correlation between average mode size of early-middle MIS 3 loess at Mobarakabad (unit 4), Toshan, Now Deh, and Neka-Abelou with the geographical latitude of the sections (**Figure 6**) in northern Iran is in agreement with the findings of Kehl et al. (2021), who suggested dust transport by north to northeasterly winds supplying coarse-grained dust to the NILP and finer facies along the NFAM. Currently, north to northeasterly winds are most frequent during late autumn and winter as the influence of the Siberian high-pressure cell intensifies (Kehl et al., 2021). Hence, similar wind dynamics during early-middle MIS 3, almost certainly, would have been responsible for the entrainment of coarse silt from the north and the transport of this coarse sediment to NFAM. However, the influence of source distance or local source activation complicates this possibility.

In contrast to the relatively fine-grained loess at Mobarakabad, the average median particle size of the Aghband loess in NLIP is

around 33–38 μm (**Figure 5**), as reported in the study of Lauer et al. (2017a). Kehl (2010) indicated the fining trend of loess from north to south and east to west across northern Iran. Also, the U-ratios of Aghband show values of 2.5–7 (Lauer et al., 2017a) and are indicative of significantly coarser silt dominance than shown in the C horizons of Mobarakabad, with a maximum of 1.3 at Mobarakabad. This difference may again partly reflect the influence of nearby source areas of especially coarse silt and also hint at the transport of dust from the north to northeast.

However, one factor must be considered when interpreting the particle size distributions of fine-grained loess such as at Mobarakabad. Similar particle size distributions to those of the loess–paleosol sequences from Mobarakabad can be seen in Miocene–Pliocene Chinese Red Clay and the parna/loessic clay of Australia (Dare-Edwards, 1984; Xu et al., 2015). In the case of Australian parna, clay size particles are likely transported as aggregates by low-level winds and not via high-altitude suspension clouds (Dare-Edwards, 1984). In China, the Red Clay sequences of the Chinese Loess Plateau have an uncertain or mixed source, but patterns in grain size variability over the depositional area suggest low-level atmospheric transport (Xu et al., 2014). As such, it is hard to use the particle size distribution of these deposits to infer transport mode, and this may also be the case in the NFAM; sediment size and availability in proximal source regions may be a more significant factor on overall distributions.

An Abrupt Shift in Dust Source and Drought Event in Unit 5

As discussed in *Particle Size Parameters of Loess Units*, the C horizon of unit 5 with a modal particle size of 30.4 μm is much coarser than the other C horizons of the section (**Figures 4**, **5**). The inferred eolian phase timing for the C horizon of unit 5 is after 34 ka, and the thickness almost reaches 6 m. The unusual thickness, U-ratio, and GSI values that characterize this unit suggest that the loess was deposited at high accumulation rates in relatively dry and windy conditions, or during a phase with a high availability of relatively coarse sediment in source regions. From this, we infer that the primary loess source for this unit was likely nearby and/or that winds were stronger in this region with more sediment availability during the time of eolian transport than during the deposition time of the C horizon of unit 4 (between 48.9 and 46.8 ka). As discussed in *Comparison With Other Northern Iranian and Global Loess Records*, the U-ratio and GSI values of the C horizon of unit 4 (**Figure 2C**) during middle MIS 3 suggest that loess accumulation at the time of unit 4 formation was mainly controlled by northerly transport winds, probably under Siberian high-pressure cell influence. In contrast, the significant increase in GSI and U-ratio of unit 5 (**Figure 2C**) which accumulated after 34 ka suggests spatiotemporal changes in sedimentary environment related to the local source or transport conditions. Indeed, the PSD of the C horizon of unit 5 at Mobarakabad is significantly coarser than all other units at the section. We therefore suggest that it may reflect the temporary activation of a local source of loess from alluvial plains of Gorgan, Atrek, and other rivers (**Figure 1A**), which originate from the nearby mountains (*Hf-Nd isotopic compositions in units 4–6*). Similar temporary close by source activation has also been seen in some Chinese loess sections and is also reflected in a dramatic increase in loess grain size (Stevens et al., 2013).

We therefore postulate that this EDP in the C horizon of unit 5 indicates an apparent shift to a likely local source and stronger wind dynamics (high GSI and U-ratio (**Figure 2C**)), almost certainly a result of spring–summer winds which dominate for a longer period in the year and eolian deposition keeping ahead of pedogenesis. Also, the EDP in the C horizon of unit 5 is generally associated with a severe drought as evidenced by high $\delta^{13}C_{bc}$ values (**Figure 2A**). This finding is in accordance with a possible drought phase that likely extended to Central Asia, as evidenced by thick loess deposits in Tajikistan and Kazakhstan allocated to MIS 4–2 (last Pleniglacial) (Mestdagh et al., 1999; Dodonov et al., 2006; Machalett et al., 2008; Fitzsimmons et al., 2018).

Hf-Nd Isotopic Compositions in Units 4–6

The $^{176}Hf/^{177}Hf$ and $^{143}Nd/^{144}Nd$ ratios (plotted as εNd (0) and εHf (0)) of clay-sized fractions from the samples are shown in **Figure 8** and **Table 1**. Clay-sized fractions from Bt and Bk horizons of the modern soil (unit 6) have εNd values of −7.18 and −7.37, respectively. The εHf value of the Bt horizon of the modern soil is −0.52, and the Bk horizon of the modern soil has an εHf value of 0.03. The C horizons of unit 5 have the most radiogenic εNd values (−6.73) of samples, and the εHf value of this horizon is −0.42. The least radiogenic εNd and εHf values (−8.06 and −0.64, respectively) are obtained from the paleosol (Bkb horizon) of unit 4. The Hf-Nd isotope data of samples (**Figure 8A**) plot well above the terrestrial array (Vervoort et al., 2011) and clay-sized array (Zhao et al., 2014), which are also above typical published zircon free arrays. Zircons are enriched in Hf and have a low εHf value compared to the average continental crust (Bayon et al., 2009). Zircons in loess will be very fine, but probably, much of the zircon is not <2 μm; the fraction we have analyzed. Also, the wind will tend to sort grains by density, so that relatively more zircon is left behind and hence depleted in the bulk samples of loess to begin with.

The samples at Mobarakabad comprise of much more radiogenic εNd (0) and εHf(0) than last glacial loess and modern and last glacial dust samples of N. America, W. Africa, Greenland, and Europe but are fairly close to some N African and some CLP samples, albeit more radiogenic (references shown in **Figure 8B**). Furthermore, the Hf-Nd isotopic values of the Asian dust end-members are $-10.8 < \varepsilon Nd < -9$ and $2.5 < \varepsilon Hf <. -4$ (Patchett et al., 1984), and similar ranges were reported for Hf-Nd isotope data from the Taklimakan, Badain Jaran, and adjacent Tengger deserts (Zhao et al., 2014). Also, Chauvel et al. (2014) reported $-10 < \varepsilon Nd < -9$ for Chashmanigar loess deposits in Tajikistan. In addition, while the εNd of Chinese, Tajik, and Central European loess sediments scatters closely around the average Nd isotopic signature of the upper continental crust [εNd (0): 10.3] (Chauvel et al., 2014;

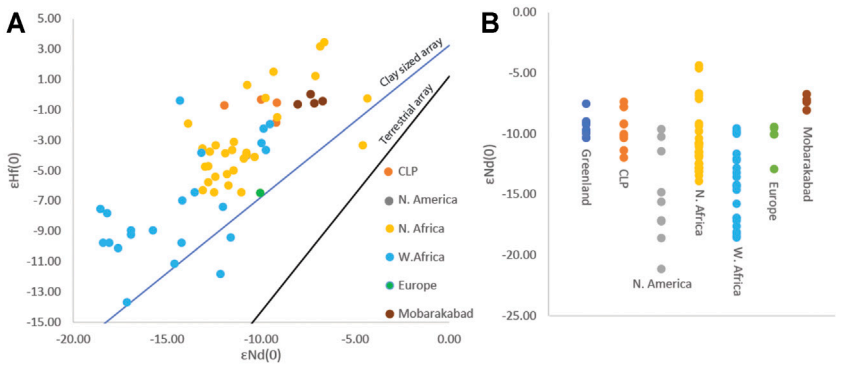

FIGURE 8 | (A) Plot of clay-sized εHf(0) vs. εNd(0) from this study (Mobarakabad) plus a range of published modern and last glacial loess and dust data from the CLP, N. America, N. Africa, W. Africa, and Europe relative to the Terrestrial array (Vervoort et al., 2011) and clay-sized array (Zhao et al., 2014). **(B)** Plot of εNd(0) by area representing more radiogenic Nd in Mobarakabad than loess and dust in Europe, W. Africa, N. America, and last glacial maximum dust in Greenland, but close to some N. African and some CLP samples. Source data are from Biscaye et al. (1997) and Svensson et al. (2000) for Greenland; Biscaye et al. (1997), Feng et al. (2009), Újvári et al. (2015), and Zhao et al. (2015) for Asia; Biscaye et al. (1997) and Újvári et al. (2015) for North America; Zhao et al. (2018) and Skonieczny et al. (2013) for North and West Africa; and Újvári et al. (2015) and Biscaye et al. (1997) for Europe.

TABLE 1 | Hf and Nd isotopic compositions of samples from Mobarakabad.

Horizon/unit	$^{143}Nd/^{144}Nd$	2δ	εNd	2δ	$^{176}Hf/^{177}Hf$	2δ	εHf	2δ
Bt horizon of modern soil (unit 6)	0.512262	4	−7.18	0.078029	0.282769	4	−0.56	0.14145
Bk horizon of modern soil (unit 6)	0.512252	16	−7.37	0.312116	0.282786	4	0.03	0.14145
C horizon of unit 5	0.512285	19	−6.73	0.370638	0.282773	5	−0.42	0.176813
Bk horizon (paleosol) of unit 4	0.512217	12	−8.06	0.234087	0.282767	4	−0.64	0.14145

[1]Errors on $^{176}Hf/^{177}Hf$ and $^{143}Nd/^{144}Nd$ represent within-run uncertainty calculated as 2σ ×10^{-6}, expressed as variation in the 6th decimal place.
[2]εHf and εNd values are calculated using the chondritic values of $^{176}Hf/^{177}Hf$ = 0.282785 and $^{143}Nd/^{144}Nd$ = 0.512630 (Bouvier et al., 2008). Measured values for BCR-2, from Weis et al. (2006, 2007), are 0.512634 ± 0.000012 for $^{143}Nd/^{144}Nd$ and 0.282857 ± 0.000004 for $^{176}Hf/^{177}Hf$.

Ujvari et al., 2018), reflecting various mixed, homogenized crustal sources, the more radiogenic εNd values of unit 4–6 at Mobarakabad range from −8.06 to −6.73 (**Figure 8B**). Hence, we propose that the more radiogenic εNd of loessic C horizon of unit 5 at Mobarakabad reflects sourcing from the relatively young crust, and the effects of incorporation of radiogenic Hf into clays released during silicate weathering. This implies that the EDP after 34 ka (unit 5) at Mobarakabad is likely sourced from a young, actively weathering crustal source, rather than from (Central) Asian dust. Hence, we presume non-glacial erosion of the tectonically close by active mountains (Alborz and Kopet Dagh) produced fine silt-sized sediment in the area which was then carried into dry basins by fluvial transport of seasonal rivers, where it is deflated as dust to form loess.

SUMMARY AND CONCLUSIONS

Our results yield new insights on the provenance and paleoclimatic implications for loess deposits in northern Iran. The most important result from particle size trends and isotopic signatures of bulk carbonates at the Mobarakabad is that the eolian deposition phase after 34 ka reflects rapid loess accumulation during severe drought associated with windy conditions and potentially activation of close by sediment sources. The different trends of $\delta^{13}C_{bc}$ and $\delta^{18}O_{bc}$ in the modern soil in comparison to paleosols suggest that the regional climate of the northern foothills of the Alborz Mountain range during the Holocene is drier than that of the late Pleistocene. In unit 1, a ~5.5‰ increase in the $\delta^{18}O_{bc}$ and $\delta^{18}O_{pc}$ values of the Btb and Btkb horizons compared to the lower Bkb and BCb horizons may reflect high rainfall (most probably during MIS 5e) in the winters, followed by dry and hot summers in which evaporative soil water loss predominates with little meteoric recharge. This would result in enriched $\delta^{18}O$ values of carbonate in the upper horizons (Btb and Btkb) of unit 1. The compiled dataset from northern Iranian loess plateau, Chinese loess plateau, and loess–paleosol sequences in Hungary suggests that $\delta^{13}C_{bc}$ and $\delta^{18}O_{bc}$ variation in loessic modern soils and paleosols most likely reflects regional precipitation change and can provide valuable, quantitative paleoenvironmental information. Particle size distributions data suggest that the depositional patterns of loess at Mobarakabad are comparable to those of loess at other sites in the northern foothills of the Alborz Mountain range. Finally, based on Hf and Nd isotopic data, we hypothesize that loess unit 5, accumulated after 34 ka at Mobarakabad, might originate from the actively eroding crustal sources of relatively young mountain (Alborz and Kopet Dagh) belts around the loess area.

DATA AVAILABILITY STATEMENT

The raw data supporting the conclusion of this article will be made available by the authors, without undue reservation.

AUTHOR CONTRIBUTIONS

AG, HT, and FK (supervisor) initialized the project and collected samples for the analysis. XM carried out the isotope measurements. TS mentored AG in clay-sized Nd-Hf isotopes and particle size interpretations and had significant contributions to the editing and revision of this work. AG wrote the manuscript, and all coauthors contributed to the article and approved the submitted version.

ACKNOWLEDGMENTS

This study is part of the Ph.D. thesis done at Gorgan University of Agricultural Sciences and Natural Resources, Iran. Wancang Zhao is thanked for providing clay-sized Hf-Nd isotopes and Bradley A. Miller for his help in determining the particle size distributions. We also gratefully thank Jef Vandenberghe and Joseph A. Mason for their highly constructive feedback that enhanced the presentation and clarity of this article.

REFERENCES

Aciego, S. M., Bourdon, B., Lupker, M., and Rickli, J. (2009). A New Procedure for Separating and Measuring Radiogenic Isotopes (U, Th, Pa, Ra, Sr, Nd, Hf) in Ice Cores. *Chem. Geology.* 266 (3–4), 194–204. doi:10.1016/j.chemgeo.2009.06.003

Amundson, R. G., Chadwick, O. A., Sowers, J. M., and Doner, H. E. (1988). Relationship between Climate and Vegetation and the Stable Carbon Isotope Chemistry of Soils in the Eastern Mojave Desert, Nevada. *Quat. Res.* 29, 245–254. doi:10.1016/0033-5894(88)90033-6

Antoine, P., Rousseau, D.-D., Moine, O., Kunesch, S., Hatté, C., Lang, A., et al. (2009). Rapid and Cyclic Aeolian Deposition during the Last Glacial in European Loess: a High-Resolution Record from Nussloch, Germany. *Quat. Sci. Rev.* 28, 2955–2973. doi:10.1016/j.quascirev.2009.08.001

Bayat, O., Karimi, A., and Khademi, H. (2017). Stable Isotope Geochemistry of Pedogenic Carbonates in Loess-Derived Soils of Northeastern Iran: Paleoenvironmental Implications and Correlation across Eurasia. *Quat. Int.* 429, 52–61. doi:10.1016/j.quaint.2016.01.040

Bayon, G., Burton, K. W., Soulet, G., Vigier, N., Dennielou, B., Etoubleau, J., et al. (2009). Hf and Nd Isotopes in marine Sediments: Constraints on Global Silicate Weathering. *Earth Planet. Sci. Lett.* 277, 318–326. doi:10.1016/j.epsl.2008.10.028

Beuselinck, L., Govers, G., Poesen, J., Degraer, G., and Froyen, L. (1998). Grain-size Analysis by Laser Diffractometry: Comparison with the Sieve-Pipette Method. *Catena* 32, 193–208. doi:10.1016/S0341-8162(98)00051-4

Biscaye, P. E., Grousset, F. E., Revel, M., Van der Gaast, S., Zielinski, G. A., Vaars, A., et al. (1997). Asian Provenance of Glacial Dust (Stage 2) in the Greenland Ice Sheet Project 2 Ice Core, Summit, Greenland. *J. Geophys. Res.* 102 (C12), 26765–26781. doi:10.1029/97jc01249

Bouvier, A., Vervoort, J. D., and Patchett, P. J. (2008). The Lu-Hf and Sm-Nd Isotopic Composition of CHUR: Constraints from Unequilibrated Chondrites and Implications for the Bulk Composition of Terrestrial Planets. *Earth Planet. Sci. Lett.* 273, 48–57. doi:10.1016/j.epsl.2008.06.010

Breecker, D. O., Sharp, Z. D., and McFadden, L. D. (2009). Seasonal Bias in the Formation and Stable Isotopic Composition of Pedogenic Carbonate in Modern Soils from central New Mexico, USA. *Geol. Soc. America Bull.* 121, 630–640. doi:10.1130/B26413.1

Burgener, L., Huntington, K. W., Hoke, G. D., Schauer, A., Ringham, M. C., Latorre, C., et al. (2016). Variations in Soil Carbonate Formation and Seasonal Bias over >4 Km of Relief in the Western Andes (30°S) Revealed by Clumped Isotope Thermometry. *Earth Planet. Sci. Lett.* 441, 188–199. doi:10.1016/j.epsl.2016.02.033

Candy, I., Adamson, K., Gallant, C. E., Whitfield, E., and Pope, R. (2012). Oxygen and Carbon Isotopic Composition of Quaternary Meteoric Carbonates from Western and Southern Europe: Their Role in Palaoenvironmental Reconstruction. *Palaeogeogr. Palaeoclimatol. Palaeoecol.* 326-328, 1–11. doi:10.1016/j.palaeo.2011.12.017

Cerling, T. E., and Quade, J. (1993). Stable Carbon and Oxygen Isotopes in Soil Carbonates. *Geophys. Monogr.* 78, 217–231. doi:10.1029/GM078p0217

Cerling, T. E., Quade, J., Wang, Y., and Bowman, J. R. (1989). Carbon Isotopes in Soils and Palaeosols as Ecology and Palaeoecology Indicators. *Nature* 341 (6238), 138–139. doi:10.1038/341138a0

Chauvel, C., Garçon, M., Bureau, S., Besnault, A., Jahn, B.-M., and Ding, Z. (2014). Constraints from Loess on the Hf-Nd Isotopic Composition of the Upper continental Crust. *Earth Planet. Sci. Lett.* 388, 48–58. doi:10.1016/j.epsl.2013.11.045

Dare-Edwards, A. J. (1984). Aeolian Clay Deposits of South-Eastern Australia: Parna or Loessic Clay? *Trans. Inst. Br. Geogr.* 9, 337–344. doi:10.2307/622237

Dever, L., Fontes, J. C., and Riché, G. (1987). Isotopic Approach to Calcite Dissolution and Precipitation in Soils under Semi-arid Conditions. *Chem. Geology. Isotope Geosci. section* 66, 307–314. doi:10.1016/0168-9622(87)90050-9

Diaz, N., King, G. E., Valla, P. G., Herman, F., and Verrecchia, E. P. (2016). Pedogenic Carbonate Nodules as Soil Time Archives: Challenges and Investigations Related to OSL Dating. *Quat. Geochronol.* 36, 120–133. doi:10.1016/j.quageo.2016.08.008

Diefendorf, A. F., Mueller, K. E., Wing, S. L., Koch, P. L., and Freeman, K. H. (2010). Global Patterns in Leaf 13C Discrimination and Implications for Studies of Past and Future Climate. *Proc. Natl. Acad. Sci.* 107 (13), 5738–5743. doi:10.1073/pnas.0910513107

Dietrich, F., Diaz, N., Deschamps, P., Ngounou Ngatcha, B., Sebag, D., and Verrecchia, E. P. (2017). Origin of Calcium in Pedogenic Carbonate Nodules from Silicate Watersheds in the Far North Region of Cameroon: Respective Contribution of *In Situ* Weathering Source and Dust Input. *Chem. Geology.* 460, 54–69. doi:10.1016/j.chemgeo.2017.04.015

Ding, Z. L., Derbyshire, E., Yang, S. L., Sun, J. M., and Liu, T. S. (2005). Stepwise Expansion of Desert Environment across Northern China in the Past 3.5 Ma and Implications for Monsoon Evolution. *Earth Planet. Sci. Lett.* 237, 45–55. doi:10.1016/j.epsl.2005.06.036

Dodonov, A. E., Sadchikova, T. A., Sedov, S. N., Simakova, A. N., and Zhou, L. P. (2006). Multidisciplinary Approach for Paleoenvironmental Reconstruction in Loess-Paleosol Studies of the Darai Kalon Section, Southern Tajikistan. *Quat. Int.* 152-153, 48–58. doi:10.1016/j.quaint.2005.12.001

Dworkin, S. I., Nordt, L., and Atchley, S. (2005). Determining Terrestrial Paleotemperatures Using the Oxygen Isotopic Composition of Pedogenic Carbonate. *Earth Planet. Sci. Lett.* 237 (1-2), 56–68. doi:10.1016/j.epsl.2005.06.054

Feng, J.-L., Zhu, L.-P., Zhen, X.-L., and Hu, Z.-G. (2009). Grain Size Effect on Sr and Nd Isotopic Compositions in Eolian Dust: Implications for Tracing Dust Provenance and Nd Model Age. *Geochem. J.* 43, 123–131. doi:10.2343/geochemj.1.0007

Fenn, K., Durcan, J. A., Thomas, D. S. G., and Banak, A. (2020). A 180 Ka Record of Environmental Change at Erdut (Croatia): a New Chronology for the Loess-Palaeosol Sequence and its Implications for Environmental Interpretation. *J. Quat. Sci* 35 (4), 582–593. doi:10.1002/jqs.3201

Fischer-Femal, B. J., and Bowen, G. J. (2021). Coupled Carbon and Oxygen Isotope Model for Pedogenic Carbonates. *Geochimica et Cosmochimica Acta* 294, 126–144. doi:10.1016/j.gca.2020.10.022

Fitzsimmons, K. E., Nowatzki, M., Dave, A. K., and Harder, H. (2020). Intersections between Wind Regimes, Topography and Sediment Supply:

Perspectives from Aeolian Landforms in Central Asia. *Palaeogeogr. Palaeoclimatol. Palaeoecol.* 540, 109531. doi:10.1016/j.palaeo.2019.109531

Fitzsimmons, K. E., Sprafke, T., Zielhofer, C., Günter, C., Deom, J.-M., Sala, R., et al. (2018). Loess Accumulation in the Tian Shan piedmont: Implications for Palaeoenvironmental Change in Arid Central Asia. *Quat. Int.* 469, 30–43. doi:10.1016/j.quaint.2016.07.041

Forman, S. L., Marín, L., Gomez, J., and Pierson, J. (2008). Late Quaternary Eolian Sand Depositional Record for Southwestern Kansas: Landscape Sensitivity to Droughts. *Palaeogeogr. Palaeoclimatol. Palaeoecol.* 265 (1-2), 107–120. doi:10.1016/j.palaeo.2008.04.028

Forman, S. L., Wright, D. K., and Bloszies, C. (2014). Variations in Water Level for Lake Turkana in the Past 8500 Years Near Mt. Porr, Kenya and the Transition from the African Humid Period to Holocene Aridity. *Quat. Sci. Rev.* 97, 84–101. doi:10.1016/j.quascirev.2014.05.005

Frechen, M., Kehl, M., Rolf, C., Sarvati, R., and Skowronek, A. (2009). Loess Chronology of the Caspian lowland in Northern Iran. *Quat. Int.* 198, 220–233. doi:10.1016/j.quaint.2008.12.012

Gallagher, T. M., and Sheldon, N. D. (2016). Combining Soil Water Balance and Clumped Isotopes to Understand the Nature and Timing of Pedogenic Carbonate Formation. *Chem. Geology.* 435, 79–91. doi:10.1016/j.chemgeo.2016.04.023

Gallant, C. E., Candy, I., van den Bogaard, P., Silva, B. N., and Turner, E. (2014). Stable Isotopic Evidence for Middle Pleistocene Environmental Change from a Loess-Paleosol Sequence: Kärlich, Germany. *Boreas* 43 (4), 818–833. doi:10.1111/bor.12065

Ghafarpour, A., Khormali, F., Balsam, W., Forman, S. L., Cheng, L., and Song, Y. (2021). The Formation of Iron Oxides and Magnetic Enhancement Mechanisms in Northern Iranian Loess-Paleosol Sequences: Evidence from Diffuse Reflectance Spectrophotometry and Temperature Dependence of Magnetic Susceptibility. *Quat. Int.* 589, 68–82. doi:10.1016/j.quaint.2021.02.019

Ghafarpour, A., Khormali, F., Balsam, W., Karimi, A., and Ayoubi, S. (2016). Climatic Interpretation of Loess-Paleosol Sequences at Mobarakabad and Aghband, Northern Iran. *Quat. Res.* 86, 95–109. doi:10.1017/s0033589400039740

Ghafarpour, A., Khormali, F., and Forman, S. L. (2017). "The OSL Chronology of the Loess- Paleosol Sequence Mobarakabad, Northern Iran," in LoessFest2017, Gorgan, Iran, 08-12 October, 68–69.

Hough, B. G., Fan, M., and Passey, B. H. (2014). Calibration of the Clumped Isotope Geothermometer in Soil Carbonate in Wyoming and Nebraska, USA: Implications for Paleoelevation and Paleoclimate Reconstruction. *Earth Planet. Sci. Lett.* 391, 110–120. doi:10.1016/j.epsl.2014.01.008

Huth, T. E., Cerling, T. E., Marchetti, D. W., Bowling, D. R., Ellwein, A. L., and Passey, B. H. (2019). Seasonal Bias in Soil Carbonate Formation and its Implications for Interpreting High-Resolution Paleoarchives: Evidence from Southern Utah. *J. Geophys. Res. Biogeosci.* 124 (3), 616–632. doi:10.1029/2018jg004496

Jacobs, P. M., and Mason, J. A. (2007). Late Quaternary Climate Change, Loess Sedimentation, and Soil Profile Development in the central Great Plains: a Pedosedimentary Model. *Geol. Soc. America Bull.* 119, 462–475. doi:10.1130/b25868.1

Kehl, M. (2010). *Quaternary Loesses, Loess-like Sediments, Soils and Climate Change in Iran*. Stuttgart, Germany: Gebrüder Borntraeger Verlagsbuchhandlung.

Kehl, M., Sarvati, R., Ahmadi, H., Frechen, M., and Skowronek, A. (2005). Loess Paleosoil-Sequences along a Climatic Gradient in Northern Iran. *E&g Quat. Sci. J.* 55, 149–173. doi:10.3285/eg.55.1.08

Kehl, M., Vlaminck, S., Köhler, T., Laag, C., Rolf, C., Tsukamoto, S., et al. (2021). Pleistocene Dynamics of Dust Accumulation and Soil Formation in the Southern Caspian Lowlands - New Insights from the Loess-Paleosol Sequence at Neka-Abelou, Northern Iran. *Quat. Sci. Rev.* 253, 106774. doi:10.1016/j.quascirev.2020.106774

Kelson, J. R., Huntington, K. W., Breecker, D. O., Burgener, L. K., Gallagher, T. M., Hoke, G. D., et al. (2020). A Proxy for All Seasons? A Synthesis of Clumped Isotope Data from Holocene Soil Carbonates. *Quat. Sci. Rev.* 234, 106259. doi:10.1016/j.quascirev.2020.106259

Khormali, F., and Kehl, M. (2011). Micromorphology and Development of Loess-Derived Surface and Buried Soils along a Precipitation Gradient in Northern Iran. *Quat. Int.* 234, 109–123. doi:10.1016/j.quaint.2010.10.022

Khormali, F., Shahriari, A., Ghafarpour, A., Kehl, M., Lehndorff, E., and Frechen, M. (2020). Pedogenic Carbonates Archive Modern and Past Precipitation Change - A Transect Study from Soils and Loess-Paleosol Sequences from Northern Iran. *Quat. Int.* 552, 79–90. doi:10.1016/j.quaint.2019.12.011

Kim, S.-T., and O'Neil, J. R. (1997). Equilibrium and Nonequilibrium Oxygen Isotope Effects in Synthetic Carbonates. *Geochimica et Cosmochimica Acta* 61 (16), 3461–3475. doi:10.1016/s0016-7037(97)00169-5

Koeniger, P., Barta, G., Thiel, C., Bajnóczi, B., Novothny, Á., Horváth, E., et al. (2014). Stable Isotope Composition of Bulk and Secondary Carbonates from the Quaternary Loess-Paleosol Sequence in Süttő, Hungary. *Quat. Int.* 319, 38–49. doi:10.1016/j.quaint.2012.06.038

Kohn, M. J. (2010). Carbon Isotope Compositions of Terrestrial C3 Plants as Indicators of (Paleo)ecology and (Paleo)climate. *Proc. Natl. Acad. Sci.* 107 (46), 19691–19695. doi:10.1073/pnas.1004933107

Költringer, C., Stevens, T., Bradák, B., Almqvist, B., Kurbanov, R., Snowball, I., et al. (2020). Enviromagnetic Study of Late Quaternary Environmental Evolution in Lower Volga Loess Sequences, Russia. *Quat. Res.* 103, 1–25. doi:10.1017/qua.2020.73

Konert, M., and Vandenberghe, J. (1977). Comparison of Laser Grain Size Analysis With Pipette and Sieve Analysis: A Solution for the Underestimation of the Clay Fraction. *Sedimentology* 44, 523–535. doi:10.1046/j.1365-3091.1997.d01-38.x

Lauer, T., Frechen, M., Vlaminck, S., Kehl, M., Lehndorff, E., Shahriari, A., et al. (2017b). Luminescence-chronology of the Loess Palaeosol Sequence Toshan, Northern Iran - A Highly Resolved Climate Archive for the Last Glacial-Interglacial Cycle. *Quat. Int.* 429, 3–12. doi:10.1016/j.quaint.2015.03.045

Lauer, T., Vlaminck, S., Frechen, M., Rolf, C., Kehl, M., Sharifi, J., et al. (2017a). The Agh Band Loess-Palaeosol Sequence - A Terrestrial Archive for Climatic Shifts during the Last and Penultimate Glacial-Interglacial Cycles in a Semiarid Region in Northern Iran. *Quat. Int.* 429, 13–30. doi:10.1016/j.quaint.2016.01.062

Lechler, A. R., Huntington, K. W., Breecker, D. O., Sweeney, M. R., and Schauer, A. J. (2018). Loess-paleosol Carbonate Clumped Isotope Record of Late Pleistocene-Holocene Climate Change in the Palouse Region, Washington State, USA. *Quat. Res.* 90 (2), 331–347. doi:10.1017/qua.2018.47

Liu, W., Yang, H., Sun, Y., and Wang, X. (2011). $\delta^{13}C$ Values of Loess Total Carbonate: a Sensitive Proxy for Asian Summer Monsoon in Arid Northwestern Margin of the Chinese Loess Plateau. *Chem. Geol.* 284 (3–4), 317–322. doi:10.1016/j.chemgeo.2011.03.011

Luo, X., Wang, H., An, Z., Zhang, Z., and Liu, W. (2020). Carbon and Oxygen Isotopes of Calcified Root Cells, Carbonate Nodules and Total Inorganic Carbon in the Chinese Loess-Paleosol Sequence: The Application of Paleoenvironmental Studies. *J. Asian Earth Sci.* 201, 104515. doi:10.1016/j.jseaes.2020.104515

Lupker, M., Aciego, S. M., Bourdon, B., Schwander, J., and Stocker, T. F. (2010). Isotopic Tracing (Sr, Nd, U and Hf) of continental and marine Aerosols in an 18th century Section of the Dye-3 Ice Core (Greenland). *Earth Planet. Sci. Lett.* 295, 277–286. doi:10.1016/j.epsl.2010.04.010

Machalett, B., Oches, E. A., Frechen, M., Zöller, L., Hambach, U., Mavlyanova, N. G., et al. (2008). Aeolian dust dynamics in Central Asia during the Pleistocene e driven by the long-termmigration, seasonality and permanency of the Asiatic polar front. *Geochem. Geophys. Geosyst.* 8, Q08Q09. doi:10.1029/2007GC001938

Marković, S. B., Hambach, U., Stevens, T., Jovanović, M., O'Hara-Dhand, K., Basarin, B., et al. (2013). Loess in the Vojvodina Region (Northern Serbia): an Essential Link between European and Asian Pleistocene Environments. *Neth. J. Geosciences* 91 (1-2), 173–188.

Mason, J. A., Greene, R. S. B., and Joeckel, R. M. (2011b). Laser Diffraction Analysis of the Disintegration of Aeolian Sedimentary Aggregates in Water. *Catena* 87, 107–118. doi:10.1016/j.catena.2011.05.015

Mason, J. A., Jacobs, P. M., Hanson, P. R., Miao, X., and Goble, R. J. (2003). Sources and Paleoclimatic Significance of Holocene Bignell Loess, Central Great Plains, USA. *Quat. Res.* 60 (3), 330–339. doi:10.1016/j.yqres.2003.07.005

Mason, J. A., Nater, E. A., Zanner, C. W., and Bell, J. C. (1999). A New Model of Topographic Effects on the Distribution of Loess. *Geomorphology* 28, 223–236. doi:10.1016/s0169-555x(98)00112-3

Mason, J. A., Swinehart, J. B., Hanson, P. R., Loope, D. B., Goble, R. J., Miao, X., et al. (2011). Late Pleistocene Dune Activity in the central Great Plains, USA. *Quat. Sci. Rev.* 30, 3858–3870. doi:10.1016/j.quascirev.2011.10.005

Mason, J. A. (2001). Transport Direction of Peoria Loess in Nebraska and Implications for Loess Sources on the central Great Plains. *Quat. Res.* 56, 79–86. doi:10.1006/qres.2001.2250

McDonald, E. V., and McFadden, L. D. (1994). "Quaternary Stratigraphy of the Providence Mountains piedmont and Preliminary Age Estimates and Regional Stratigraphic Correlations of Quaternary Deposits in the Eastern Mojave Desert, California," in *Geological Investigations of an Active Margin. Geol. Soc. Am. Cordilleran Sect. Fieldtrip Guideb*. Editors S. F. McGill and T. M. Ross, 205–210.

Mestdagh, H., Haesaerts, P., Dodonov, A., and Hus, J. (1999). Pedosedimentary and Climatic Reconstruction of the Last Interglacial and Early Glacial Loess-Paleosol Sequence in South Tadzhikistan. *Catena* 35, 197–218. doi:10.1016/s0341-8162(98)00100-3

Miller, B. A., and Schaetzl, R. J. (2012). Precision of Soil Particle Size Analysis Using Laser Diffractometry. *Soil Sci. Soc. Am. J.* 76, 1719–1727. doi:10.2136/sssaj2011.0303

Monger, H. C., Cole, D. R., Gish, J. W., and Giordano, T. H. (1998). Stable Carbon and Oxygen Isotopes in Quaternary Soil Carbonates as Indicators of Ecogeomorphic Changes in the Northern Chihuahuan Desert, USA. *Geoderma* 82, 137–172. doi:10.1016/s0016-7061(97)00100-6

Muhs, D. R., Aleinikoff, J. N., Stafford, T. W., Jr., Kihl, R., Been, J., Mahan, S. A., et al. (1999). Late Quaternary Loess in Northeastern Colorado: Part I-Age and Paleoclimatic Significance. *Geol. Soc. Am. Bull.* 111, 1861–1875. doi:10.1130/0016-7606(1999)111<1861:lqlinc>2.3.co;2

Muhs, D. R., Bettis, E. A., Aleinikoff, J. N., McGeehin, J. P., Beann, J., Skipp, G., et al. (2008). Origin and Paleoclimatic Significance of Late Quaternary Loess in Nebraska: Evidence from Stratigraphy, Chronology, Sedimentology, and Geochemistry. *Geol. Soc. America Bull.* 120, 1378–1407. doi:10.1130/b26221.1

Muhs, D. R., Shroder, J., and Lancaster, N. (2013). "11.9 Loess and its Geomorphic, Stratigraphic, and Paleoclimatic Significance in the Quaternary," in *Treatise on Geomorphology*. *Aeolian Geomorphology*. Editors D. J. Sherman and A. C. W. Baas (San Diego, CA: Academic Press), Vol. 11, 149–183. doi:10.1016/b978-0-12-374739-6.00302-x

Nilson, E., and Lehmkuhl, F. (2001). Interpreting Temporal Patterns in the Late Quaternary Dust Flux from Asia to the North Pacific. *Quat. Int.* 76-77 (77), 67–76. doi:10.1016/s1040-6182(00)00090-2

Ning, Y. F., Liu, W. G., and An, Z. S. (2007). Variation of Soil delta C-13 Values in Xifeng Loess- Paleosol Sequence and its Paleoenvironmental Implication. *Chin. Sci. Bull.* 51, 1350–1354.

Nottebaum, V., Lehmkuhl, F., Stauch, G., Hartmann, K., Wünnemann, B., Schimpf, S., et al. (2014). Regional Grain Size Variations in Aeolian Sediments along the Transition between Tibetan highlands and north-western Chinese Deserts - the Influence of Geomorphological Settings on Aeolian Transport Pathways. *Earth Surf. Process. Landforms* 39, 1960–1978. doi:10.1002/esp.3590

Ozer, M., Orhan, M., and Isik, N. S. (2010). Effect of Particle Optical Properties on Size Distribution of Soils Obtained by Laser Diffraction. *Environ. Eng. Geosci.* 16, 163–173. doi:10.2113/gseegeosci.16.2.163

Passey, B. H., Levin, N. E., Cerling, T. E., Brown, F. H., and Eiler, J. M. (2010). High-temperature Environments of Human Evolution in East Africa Based on Bond Ordering in Paleosol Carbonates. *Proc. Natl. Acad. Sci.* 107, 11245–11249. doi:10.1073/pnas.1001824107

Patchett, P. J., White, W. M., Feldmann, H., Kielinczuk, S., and Hofmann, A. W. (1984). Hafnium/rare Earth Element Fractionation in the Sedimentary System and Crustal Recycling into the Earth's Mantle. *Earth Planet. Sci. Lett.* 69, 365–378. doi:10.1016/0012-821x(84)90195-x

Peters, N. A., Huntington, K. W., and Hoke, G. D. (2013). Hot or Not? Impact of Seasonally Variable Soil Carbonate Formation on Paleotemperature and O-Isotope Records from Clumped Isotope Thermometry. *Earth Planet. Sci. Lett.* 361, 208–218. doi:10.1016/j.epsl.2012.10.024

Pettke, T., Lee, D.-C., Halliday, A. N., and Rea, D. K. (2002). Radiogenic Hf Isotopic Compositions of continental Eolian Dust from Asia, its Variability and its Implications for Seawater Hf. *Earth Planet. Sci. Lett.* 202, 453–464. doi:10.1016/s0012-821x(02)00778-1

Polakowski, C., Sochan, A., Bieganowski, A., Ryzak, M., Földényi, R., and Tóth, J. (2014). Influence of the Sand Particle Shape on Particle Size Distribution Measured by Laser Diffraction Method. *Int. Agrophysics* 28, 195–200. doi:10.2478/intag-2014-0008

Pourmand, A., Prospero, J. M., and Sharifi, A. (2014). Geochemical Fingerprinting of Trans-Atlantic African Dust Based on Radiogenic Sr-Nd-Hf Isotopes and Rare Earth Element Anomalies. *Geology* 42, 675–678. doi:10.1130/g35624.1

Pourmasoumi, M., Khormali, F., Ayoubi, S., Kehl, M., and Kiani, F. (2019). Development and Magnetic Properties of Loess-Derived forest Soils along a Precipitation Gradient in Northern Iran. *J. Mt. Sci.* 16, 1848–1868. doi:10.1007/s11629-018-5288-4

Prins, M. A., Zheng, H., Beets, K., Troelstra, S., Bacon, P., Kamerling, I., et al. (2009). Dust Supply from River Floodplains: the Case of the Lower Huang He (Yellow River) Recorded in a Loess-Palaeosol Sequence from the Mangshan Plateau. *J. Quat. Sci.* 24, 75–84. doi:10.1002/jqs.1167

Pu, W., Gao, J., Zhao, K., Ling, H., and Jiang, S. (2005). Separation Method of Rb–Sr, Sm–Nd Using DCTA and HIBA. *J. Nanjing Univ. Natural Sci.* 4, 016.

Pye, K. (1995). The Nature, Origin and Accumulation of Loess. *Quat. Sci. Rev.* 14, 653–667. doi:10.1016/0277-3791(95)00047-x

Qiang, M., Lang, L., and Wang, Z. (2010). Do fine-grained Components of Loess Indicate Westerlies: Insights from Observations of Dust Storm Deposits at Lenghu (Qaidam Basin, China). *J. Arid Environments* 74, 1232–1239. doi:10.1016/j.jaridenv.2010.06.002

Quade, J., Breecker, D. O., Daeron, M., and Eiler, J. (2011). The Paleoaltimetry of Tibet: An Isotopic Perspective. *Am. J. Sci.* 311, 77–115. doi:10.2475/02.2011.01

Quade, J., Cerling, T. E., and Bowman, J. R. (1989). Systematic Variations in the Carbon and Oxygen Isotopic Composition of Pedogenic Carbonate along Elevation Transects in the Southern Great Basin, United States. *Geol. Soc. Am. Bull.* 101 (4), 464–475. doi:10.1130/0016-7606(1989)101<0464:svitca>2.3.co;2

Quade, J., Eiler, J., Daëron, M., and Achyuthan, H. (2013). The Clumped Isotope Geothermometer in Soil and Paleosol Carbonate. *Geochimica et Cosmochimica Acta* 105, 92–107. doi:10.1016/j.gca.2012.11.031

Quade, J., Garzione, C., and Eiler, J. (2007). Paleoelevation Reconstruction Using Pedogenic Carbonates. *Rev. Mineralogy Geochem.* 66, 53–87. doi:10.2138/rmg.2007.66.3

Rao, Z. G., Zhu, Z. Y., Chen, F. H., and Zhang, J. W. (2006). Does $\delta^{13}C_{carb}$ of the Chinese Loess Indicate Past C3/C4 Abundance? A Review of Research on Stable Carbon Isotopes of the Chinese Loess. *Quat. Sci. Rev.* 25, 22512257. doi:10.1016/j.quascirev.2006.03.013

Ringham, M. C., Hoke, G. D., Huntington, K. W., and Aranibar, J. N. (2016). Influence of Vegetation Type and Site-To-Site Variability on Soil Carbonate Clumped Isotope Records, Andean piedmont of Central Argentina (32-34°S). *Earth Planet. Sci. Lett.* 440 (June), 1–11. doi:10.1016/j.epsl.2016.02.003

Rousseau, D.-D., Antoine, P., Boers, N., Lagroix, F., Ghil, M., Lomax, J., et al. (2020). Dansgaard-Oeschger-like Events of the Penultimate Climate Cycle: the Loess point of View. *Clim. Past* 16 (2), 713–727. doi:10.5194/cp-16-713-2020

Rousseau, D.-D., Boers, N., Sima, A., Svensson, A., Bigler, M., Lagroix, F., et al. (2017). (MIS3 & 2) Millennial Oscillations in Greenland Dust and Eurasian Aeolian Records - A Paleosol Perspective. *Quat. Sci. Rev.* 169, 99–113. doi:10.1016/j.quascirev.2017.05.020

Rousseau, D.-D., Sima, A., Antoine, P., Hatté, C., Lang, A., and Zöller, L. (2007). Link between European and North-Atlantic Abrupt Climate Changes over the Last Glaciation. *Geophys. Res. Lett.* 34, L22713. doi:10.1029/2007gl031716

Rousseau, D. D., Antoine, P., Hatté, C., Lang, A., Zöller, L., Fontugne, M., et al. (2002). Abrupt Millennial Climatic Changes from Nussloch (Germany) Upper Weichselian Eolian Records during the Last Glaciation. *Quat. Sci. Rev.* 21, 1577–1582. doi:10.1016/s0277-3791(02)00034-3

Schaetzl, R. J., Forman, S. L., and Attig, J. W. (2014). Optical Ages on Loess Derived from Outwash Surfaces Constrain the advance of the Laurentide Ice Sheet Out of the Lake Superior Basin, USA. *Quat. Res.* 81 (2), 318–329. doi:10.1016/j.yqres.2013.12.003

Schubert, B. A., and Jahren, A. H. (2012). The Effect of Atmospheric CO2 Concentration on Carbon Isotope Fractionation in C3 Land Plants. *Geochimica et Cosmochimica Acta* 96, 29–43. doi:10.1016/J.GCA.2012.08.003

Shahriari, A., Khormali, F., Bläsing, M., Vlaminck, S., Kehl, M., Frechen, M., et al. (2017). Biomarkers in Modern and Buried Soils of Semi-desert and forest Ecosystems of Northern Iran. *Quat. Int.* 429, 62–73. doi:10.1016/j.quaint.2016.02.048

Sharifigarmdareh, J., Khormali, F., Scheidt, S., Rolf, C., Kehl, M., and Frechen, M. (2020). Investigating Soil Magnetic Properties with Pedogenic Variation along a

Precipitation Gradient in Loess-Derived Soils of the Golestan Province, Northern Iran. *Quat. Int.* 552, 100–110. doi:10.1016/j.quaint.2019.11.022

Shoaee, M. J., Vahdati Nasab, H., and Petraglia, M. D. (2021). The Paleolithic of the Iranian Plateau: Hominin Occupation History and Implications for Human Dispersals across Southern Asia. *J. Anthropological Archaeology* 62, 101292. doi:10.1016/j.jaa.2021.101292

Skonieczny, C., Bory, A., Bout-Roumazeilles, V., Abouchami, W., Galer, S. J. G., Crosta, X., et al. (2013). A Three-Year Time Series of mineral Dust Deposits on the West African Margin: Sedimentological and Geochemical Signatures and Implications for Interpretation of marine Paleo-Dust Records. *Earth Planet. Sci. Lett.* 364, 145–156. doi:10.1016/j.epsl.2012.12.039

Soil Survey Staff (2014). *Keys to Soil Taxonomy*. Washington, D.C., USA: U.S. Department of Agriculture, Natural Resources Conservation Service.

Song, Y., Li, Y., Cheng, L., Zong, X., Kang, S., Ghafarpour, A., et al. (2021). Spatio-temporal Distribution of Quaternary Loess across Central Asia. *Palaeogeogr. Palaeoclimatol. Palaeoecol.* 567, 110279. doi:10.1016/j.palaeo.2021.110279

Stevens, T., Adamiec, G., Bird, A. F., and Lu, H. (2013). An Abrupt Shift in Dust Source on the Chinese Loess Plateau Revealed through High Sampling Resolution OSL Dating. *Quat. Sci. Rev.* 82, 121–132. doi:10.1016/j.quascirev.2013.10.014

Stevens, T., and Lu, H. (2009). Optically Stimulated Luminescence Dating as a Tool for Calculating Sedimentation Rates in Chinese Loess: Comparisons with Grain-Size Records. *Sedimentology* 56 (4), 911–934. doi:10.1111/j.1365-3091.2008.01004.x

Stevens, T., Marković, S. B., Zech, M., Hambach, U., and Sümegi, P. (2011). Dust Deposition and Climate in the Carpathian Basin over an Independently Dated Last Glacial-Interglacial Cycle. *Quat. Sci. Rev.* 30, 662–681. doi:10.1016/j.quascirev.2010.12.011

Stevens, T., Sechi, D., Bradák, B., Orbe, R., Baykal, Y., Cossu, G., et al. (2020). Abrupt Last Glacial Dust Fall over Southeast England Associated with Dynamics of the British-Irish Ice Sheet. *Quat. Sci. Rev.* 250, 106641. doi:10.1016/j.quascirev.2020.106641

Stevenson, B. A., Kelly, E. F., McDonald, E. V., Busacca, A. J., and Welker, J. M. (2010). Oxygen Isotope Ratios in Holocene Carbonates across a Climatic Gradient, Eastern Washington State, USA: Evidence for Seasonal Effects on Pedogenic mineral Isotopic Composition. *The Holocene* 20, 575–583. doi:10.1177/0959683609356588

Sun, D., Bloemendal, J., Rea, D. K., Vandenberghe, J., Jiang, F., An, Z., et al. (2002). Grain-size Distribution Function of Polymodal Sediments in Hydraulic and Aeolian Environments, and Numerical Partitioning of Sedimentary Components. *Sediment. Geol* 152, 262–277. doi:10.1016/s0037-0738(02)00082-9

Sun, Y., Kutzbach, J., An, Z., Clemens, S., Liu, Z., Liu, W., et al. (2015). Astronomical and Glacial Forcing of East Asian Summer Monsoon Variability. *Quat. Sci. Rev.* 115, 132–142. doi:10.1016/j.quascirev.2015.03.009

Svensson, A., Biscaye, P. E., and Grousset, F. E. (2000). Characterization of Late Glacial continental Dust in the Greenland Ice Core Project Ice Core. *J. Geophys. Res.* 105 (D4), 4637–4656. doi:10.1029/1999jd901093

Sweeney, M. R., and Mason, J. A. (2013). Mechanisms of Dust Emission from Pleistocene Loess Deposits, Nebraska, USA. *J. Geophys. Res. Earth Surf.* 118, 1460–1471. doi:10.1002/jgrf.20101

Tan, H., Liu, Z., Rao, W., Jin, B., and Zhang, Y. (2017). Understanding Recharge in Soil-Groundwater Systems in High Loess hills on the Loess Plateau Using Isotopic Data. *Catena* 156, 18–29. doi:10.1016/J.CATENA.2017.03.022

Tripaldi, A., Ciccioli, P. L., Alonso, M. S., and Forman, S. L. (2010). Petrography and Geochemistry of Late Quaternary Dune fields of Western Argentina: Provenance of Aeolian Materials in Southern South America. *Aeolian Res.* 2 (1), 33–48. doi:10.1016/j.aeolia.2010.01.001

Újvári, G., Bernasconi, S. M., Stevens, T., Kele, S., Páll-Gergely, B., Surányi, G., et al. (2021). Stadial-Interstadial Temperature and Aridity Variations in East Central Europe Preceding the Last Glacial Maximum. *Paleoceanogr Paleoclimatol* 36, e2020PA004170. doi:10.1029/2020PA004170

Újvári, G., Kele, S., Bernasconi, S. M., Haszpra, L., Novothny, Á., and Bradák, B. (2019). Clumped Isotope Paleotemperatures from MIS 5 Soil Carbonates in Southern Hungary. *Palaeogeogr. Palaeoclimatol. Palaeoecol.* 518, 72–81.

Újvári, G., Kok, J. F., Varga, G., and Kovács, J. (2016). The Physics of Wind-Blown Loess: Implications for Grain Size Proxy Interpretations in Quaternary Paleoclimate Studies. *Earth. Sci. Rev.* 154, 247–278.

Újvári, G., Stevens, T., Svensson, A., Klötzli, U. S., Manning, C., Németh, T., et al. (2015). Two Possible Source Regions for central Greenland Last Glacial Dust. *Geophys. Res. Lett.* 42, 10,399–10,408.

Újvári, G., Varga, A., Ramos, F. C., Kovács, J., Németh, T., and Stevens, T. (2012). Evaluating the Use of clay Mineralogy, Sr–Nd Isotopes and Zircon U–Pb Ages in Tracking Dust Provenance: An Example from Loess of the Carpathian Basin. *Chem. Geol.* 304, 83–96.

Újvári, G., Wegner, W., Klötzli, U., Horschinegg, M., and Hippler, D. (2018). Sr-Nd-Hf Isotopic Analysis of < 10 Mg Dust Samples: Implications for Ice Core Dust Source Fingerprinting. *Geochem. Geophys. Geosyst.* 19 (1), 60–72.

Vandenberghe, J. (2013). Grain Size of fine-grained Windblown Sediment: a Powerful Proxy for Process Identification. *Earth-Science Rev.* 121, 18–30. doi:10.1016/j.earscirev.2013.03.001

Vandenberghe, J., Mücher, H. J., Roebroeks, W., and Gemke, D. (1985). Lithostratigraphy and palaeoenvironment of the Pleistocene deposits at Maastricht-Belvédère, southern Limburg, The Netherlands. *Med. Rijks Geol. Dienst.* 39, 7–18.

Vandenberghe, J., Renssen, H., Van Huissteden, K., Nugteren, G., Konert, M., Lu, H., et al. (2006). Penetration of Atlantic westerly Winds into Central and East Asia. *Quat. Sci. Rev.* 25, 2380–2389. doi:10.1016/j.quascirev.2006.02.017

Vandenberghe, J., Sun, Y., Wang, X., Abels, H. A., and Liu, X. (2018). Grain-Size Characterization of Reworked Fine-Grained Aeolian Deposits. *Earth Sci. Rev.* 177, 43–52. doi:10.1016/J.EARSCIREV.2017.11.005

Vandenberghe, J., Zhisheng, A., Nugteren, G., Huayu, L., and Van Huissteden, K. (1997). New Absolute Time Scale for the Quaternary Climate in the Chinese Loess Region by Grain-Size Analysis. *Geol* 25, 35. doi:10.1130/0091-7613(1997)025<0035:natsft>2.3.co;2

Varga, G., Gresina, F., Újvári, G., Kovács, J., and Szalai, Z. (2019b). On the Reliability and Comparability of Laser Diffraction Grain Size Measurements of Paleosols in Loess Records. *Sediment. Geology.* 389, 42–53. doi:10.1016/j.sedgeo.2019.05.011

Varga, G., Újvári, G., and Kovács, J. (2019a). Interpretation of Sedimentary (Sub)populations Extracted from Grain Size Distributions of Central European Loess-Paleosol Series. *Quat. Int.* 502, 60–70. doi:10.1016/j.quaint.2017.09.021

Vervoort, J. D., Plank, T., and Prytulak, J. (2011). The Hf-Nd Isotopic Composition of Marine Sediments. *Geochim. Cosmochim. Acta* 75, 5903–5926. doi:10.1016/j.gca.2011.07.046

Vlaminck, S., Kehl, M., Lauer, T., Shahriari, A., Sharifi, J., Eckmeier, E., et al. (2016). Loess-soil Sequence at Toshan (Northern Iran): Insights into Late Pleistocene Climate Change. *Quat. Int.* 399, 122–135. doi:10.1016/j.quaint.2015.04.028

Vlaminck, S., Kehl, M., Rolf, C., Franz, S. O., Lauer, T., Lehndorff, E., et al. (2018). Late Pleistocene Dust Dynamics and Pedogenesis in Southern Eurasia - Detailed Insights from the Loess Profile Toshan (NE Iran). *Quat. Sci. Rev.* 180, 75–95. doi:10.1016/j.quascirev.2017.11.010

Vriend, M., Prins, M. A., Buylaert, J.-P., Vandenberghe, J., and Lu, H. (2011). Contrasting Dust Supply Patterns across the north-western Chinese Loess Plateau during the Last Glacial-Interglacial Cycle. *Quat. Int.* 240, 167–180. doi:10.1016/j.quaint.2010.11.009

Wacha, L., Laag, C., Grizelj, A., Tsukamoto, S., Zeeden, C., Ivanišević, D., et al. (2021). High-resolution Palaeoenvironmental Reconstruction at Zmajevac (Croatia) over the Last Three Glacial/interglacial Cycles. *Palaeogeogr. Palaeoclimatol. Palaeoecol.* 576, 110504. doi:10.1016/j.palaeo.2021.110504

Xu, Y., Li, J., Yue, L., Jiang, J., Sun, F., and Zhang, L. (2015). Grain-size Characteristics of Red clay Deposits on the Eastern Edge of Chinese Loess Plateau and its Implications for Neogene Evolution of East Asian winter Monsoon. *Environ. Earth Sci.* 73 (11), 7445–7456. doi:10.1007/s12665-014-3918-x

Yang, S., and Ding, Z. (2008). Advance-retreat History of the East-Asian Summer Monsoon Rain- Fall belt over Northern China during the Last Two Glacial-Interglacial Cycles. *Earth Planet. Sci. Lett.* 274 (3–4), 499–510. doi:10.1016/j.epsl.2008.08.001

Yang, Y.-h., Zhang, H.-f., Chu, Z.-y., Xie, L.-w., and Wu, F.-y. (2010). Combined Chemical Separation of Lu, Hf, Rb, Sr, Sm and Nd from a Single Rock Digest and Precise and Accurate Isotope Determinations of Lu-Hf, Rb-Sr and Sm-Nd Isotope Systems Using Multi-Collector ICP-MS and TIMS. *Int. J. Mass Spectrom.* 290, 120–126. doi:10.1016/j.ijms.2009.12.011

Zamanian, K., Lechler, A. R., Schauer, A. J., Kuzyakov, Y., and Huntington, K. W. (2021). The $\delta^{13}C$, $\delta^{18}O$ and $\Delta47$ Records in Biogenic, Pedogenic and Geogenic Carbonate Types from Paleosol-Loess Sequence and Their Paleoenvironmental Meaning. *Quat. Res.* 101, 256–272.

Zeeden, C., Kels, H., Hambach, U., Schulte, P., Protze, J., Eckmeier, E., et al. (2016). Three Climatic Cycles Recorded in a Loess-Palaeosol Sequence at Semlac (Romania) - Implications for Dust Accumulation in South-Eastern Europe. *Quat. Sci. Rev.* 154, 130–142. doi:10.1016/j.quascirev.2016.11.002

Zhao, W., Balsam, W., Williams, E., Long, X., and Ji, J. (2018). Sr-Nd-Hf Isotopic Fingerprinting of Transatlantic Dust Derived from North Africa. *Earth Planet. Sci. Lett.* 486, 23–31. doi:10.1016/j.epsl.2018.01.004

Zhao, W., Sun, Y., Balsam, W., Lu, H., Liu, L., Chen, J., et al. (2014). Hf-Nd Isotopic Variability in mineral Dust from Chinese and Mongolian Deserts: Implications for Sources and Dispersal. *Sci. Rep.* 4, 5837. doi:10.1038/srep05837

Zhao, W., Sun, Y., Balsam, W., Zeng, L., Lu, H., Otgonbayar, K., et al. (2015). Clay-sized Hf-Nd-Sr Isotopic Composition of Mongolian Dust as a Fingerprint for Regional to Hemispherical Transport. *Geophys. Res. Lett.* 42, 5661–5669. doi:10.1002/2015gl064357

Conflict of Interest: The authors declare that the research was conducted in the absence of any commercial or financial relationships that could be construed as a potential conflict of interest.